

STANDARDIZATION OF MULTIVARIATE GAUSSIAN MIXTURE MODELS AND BACKGROUND ADJUSTMENT OF PET IMAGES IN BRAIN ONCOLOGY*

BY MENG LI[†] AND ARMIN SCHWARTZMAN[‡]

Rice University[†] and University of California, San Diego[‡]

In brain oncology, it is routine to evaluate the progress or remission of the disease based on the differences between a pre-treatment and a post-treatment Positron Emission Tomography (PET) scan. Background adjustment is necessary to reduce confounding by tissue-dependent changes not related to the disease. When modeling the voxel intensities for the two scans as a bivariate Gaussian mixture, background adjustment translates into standardizing the mixture at each voxel, while tumor lesions present themselves as outliers to be detected. In this paper, we address the question of how to standardize the mixture to a standard multivariate normal distribution, so that the outliers (i.e., tumor lesions) can be detected using a statistical test. We show theoretically and numerically that the tail distribution of the standardized scores is favorably close to standard normal in a wide range of scenarios while being conservative at the tails, validating voxelwise hypothesis testing based on standardized scores. To address standardization in spatially heterogeneous image data, we propose a spatial and robust multivariate expectation-maximization (EM) algorithm, where prior class membership probabilities are provided by transformation of spatial probability template maps and the estimation of the class mean and covariances are robust to outliers. Simulations in both univariate and bivariate cases suggest that standardized scores with soft assignment have tail probabilities that are either very close to or more conservative than standard normal. The proposed methods are applied to a real data set from a PET phantom experiment, yet they are generic and can be used in other contexts.

1. Introduction. In brain oncology, it is routine to evaluate the progression or remission of the disease based on differences between a pre-treatment and a post-treatment Positron Emission Tomography (PET) three-dimensional scan (Valk et al., 2003). Using markers such as injected F-18-fluorodeoxyglucose (FDG), these images measure the activity of glucose metabolism in human brains, which is normalized by dose and patient weight to standard uptake value (SUV) units.

*This work was partially supported by NIH grant R21EB13795.

Keywords and phrases: Background adjustment; PET images; Tumor detection; Multivariate Gaussian mixture model; Outlier detection; Robust EM algorithm; Spatial modeling; Standardized scores; Tail distributions; Voxelwise inference.

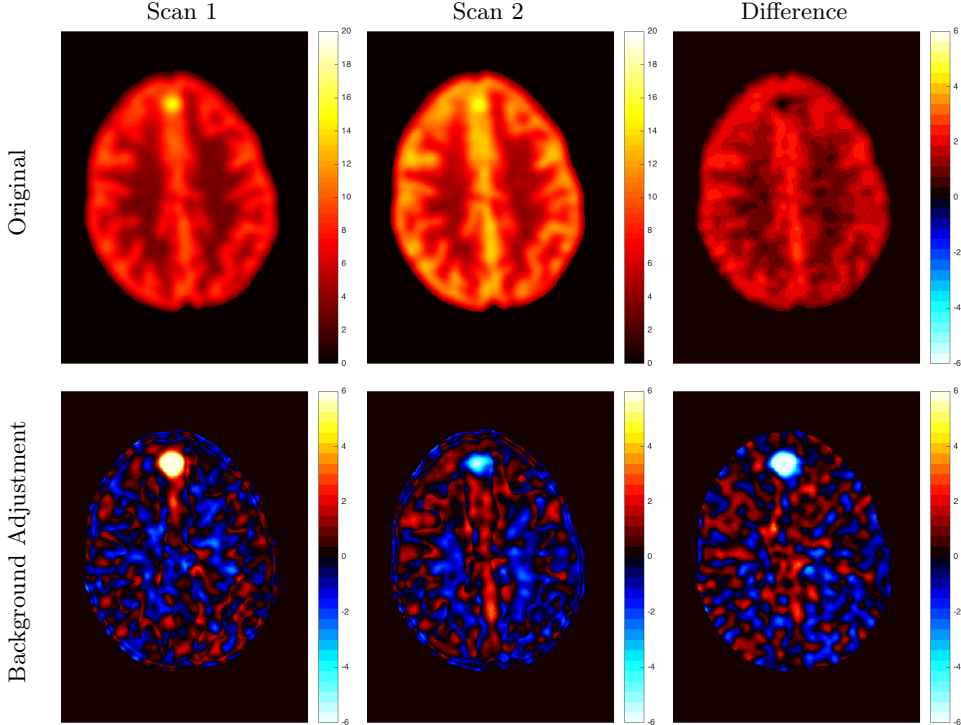
A standard practice in this setting is to conduct analyses based on differences between *scalar summaries* of the two PET scans (Young et al., 1999; Wahl et al., 2009), such as the maximum SUV, calculated within user-defined regions of interest (ROIs) (Zasadny and Wahl, 1993; Lee et al., 2009; Takeda et al., 2011). However, due to variations in scanner settings, neurological activity or pharmacological drug effects, the scans may exhibit background differences even without significant progression or remission of the disease itself (Soret et al., 2007; Bai et al., 2013; Soffientini et al., 2016). The background effect may even be spatially heterogeneous, varying according to tissue type (Guo et al., 2014; Qin et al., 2017). Moreover, lesion changes may be missed if those lesions are not included in the user-defined ROIs. For these reasons, Guo et al. (2014) proposed a new approach comparing the two PET scans *voxelwise*.

As a motivating example that will be detailed in Section 5, Figure 1 shows data from the phantom experiment in Qin et al. (2017) simulating pre- and post-treatment scans with a tumor lesion. A direct voxelwise difference between the two scans shows a global non-homogeneous background change while failing to detect changes in the lesion (Figure 1, Row 1 and Column 3). This observation suggests that *background adjustment* is necessary in voxelwise comparisons to reduce confounding by tissue-dependent changes not related to the disease, in order to isolate localized differences that are relevant to assess the disease status.

Statistical models have been intensively used in quantitative analysis for PET imaging to provide automated and objective assessment (Leahy and Qi, 2000; Borghammer et al., 2009; O’Sullivan et al., 2014). Gaussian mixture models (GMM) are one of most popular approaches (Zhang et al., 1994; Guo et al., 2014; Soffientini et al., 2016), commonly assuming that voxel intensities belong to a mixture model with three components representing gray matter (GM), white matter (WM) and cerebro-spinal fluid (CSF). This is standard, for example, in the widely used software Statistical Parametric Mapping or SPM (Ashburner and Friston, 2005; Ashburner, 2012).

Modeling the voxel intensities in the two scans as a bivariate mixture model with GM, WM and CSF components, the background adjustment procedure in Guo et al. (2014) consisted of standardizing a multivariate Gaussian mixture model at each voxel. Large localized changes, presumably representing tumors, were then detected by performing a statistical test at each voxel with respect to an empirical null distribution. Following up on that work, Qin et al. (2017) made a heuristic observation that the distribution of the standardized difference scores *across voxels* was close to standard normal, supporting the use of the standard normal as the null distribution

Fig 1: Effects of background adjustment in detecting changes in tumor lesions in a phantom study. The 1st row shows a transverse slice of the original PET scans. Their direct difference in the last column exhibits a large positive background change between the scans. The 2nd row shows the respective standardized images via background adjustment and their difference based on our proposed method detailed later.



for the voxelwise tests. From a pure frequentist perspective, however, the p-value for *each voxel* should be computed from the distribution of the standardized score at *that voxel*. [Qin et al. \(2017\)](#) offered no investigation of whether and why the distribution of the standardized scores *at each voxel*, whose standardization is imperfect and different, should be standard normal.

Motivated by the problem above, this paper addresses the question of whether the distribution of the standardized score at each voxel is close to standard normal, considering a range of challenges from realistic PET image settings with lesions present, spatial heterogeneity, and tissue dependent background changes. This comparison is most important at the tails of the distribution (one-sided or two-sided), where inference usually occurs.

In its simplest form, the question can be formulated more abstractly as follows. Suppose we have observations from a multivariate Gaussian mixture model, among which there are some outliers we wish to detect. As an illustration, Figure 2(a) shows a bivariate mixture model with some outliers that do not belong to any of the classes but also do not constitute enough data to fit a third class. Is it possible to standardize the mixture so that the distribution will be centered around the origin with identity covariance? If so, the standardized mixture represents a null distribution against which the outlying observations can be detected using a statistical test, as illustrated in Figure 2(b). But will the tails of the distribution be close enough to standard normal so that p-values for detection are valid?

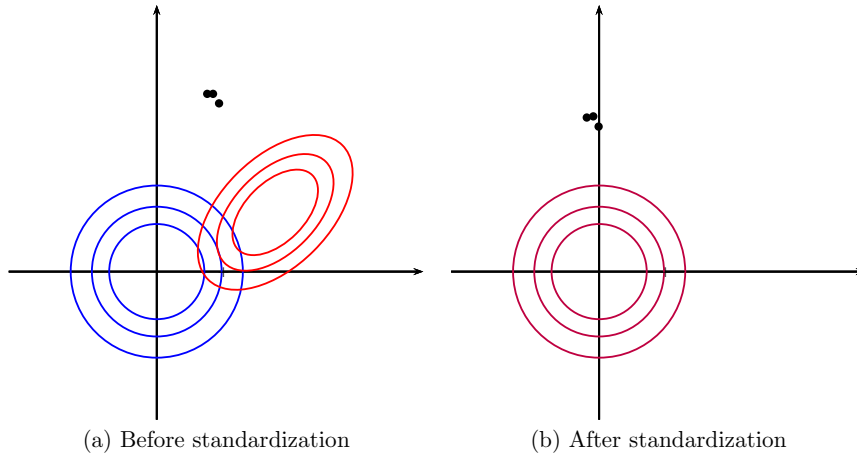


Fig 2: Standardization of a two-component bivariate Gaussian mixture model with outliers. (a) density contours at (40%, 50%, 60%)th quantiles (blue and red) of each of the two classes in the mixture (same parameters as in Figure 3 (b)). (b) density contour at (40%, 50%, 60%)th quantiles (purple) of the standardized mixture, obtained using equation (2.5) with equal membership probabilities. The black dots in (a) and (b) represent the outliers before and after standardization, respectively.

There is a rich literature on the estimation and application of finite mixture models (McLachlan and Peel, 2000), leading to numerous research areas such as the expectation-maximization (EM) algorithm (Dempster et al., 1977; Redner and Walker, 1984; Gupta and Chen, 2011), the estimation of unknown components (Richardson and Green, 1997; Vlassis and Likas, 1999; Stephens, 2000; Lo et al., 2001; Figueiredo and Jain, 2002), and mixture of general distributions other than Gaussian (Peel and McLachlan, 2000; Das-

gupta et al., 2005; Hanson, 2006; Lin et al., 2007; Venturini et al., 2008), only to name a few. However, there is limited work on inference problems such as hypothesis testing in a mixture model context.

In the first half of this paper, we study the standardization of a Gaussian mixture model systematically in various but simple ways. We show that, surprisingly, the tail distribution of the standardized scores is favorably close to standard normal in a wide range of scenarios while being conservative at the tails, making it suitable for statistical inference. Compared to the standardization method for background adjustment in Guo et al. (2014) and Qin et al. (2017), we consider several variations using both soft and hard assignment of the observations to latent classes. In the data application in Figure 1, the analysis based on the model-based standardized differences proposed in this paper is successful (Row 2 and Column 3) as the background difference is now randomly distributed around zero and the lesion change is clearly visible; see Section 5 for more details. The distributions of the corresponding standardized scores are evaluated here theoretically, numerically and via simulations. Theoretically, it is shown that the standardized scores are indeed close to standard normal under a variety of extreme parameter settings. In non-extreme parameter settings, it is shown numerically that the soft assignment methods lead to conservative tail probabilities, making them valid for hypothesis testing purposes. It is also shown that the tail probabilities are not very sensitive to the class probabilities, which is an advantage as these are hard to estimate in practice.

The second half of the paper addresses a practical challenge in analyzing PET images, namely, the standardization of Gaussian mixture models in spatially heterogeneous data. Brain images typically require using *spatial* Gaussian mixtures models, where the class membership probability varies spatially. Prior knowledge of the class membership probability at each voxel is available as templates from brain atlases (for example, SPM (Ashburner and Friston, 2005; Ashburner, 2012)). However, voxels that exhibit large changes in intensity such as lesions, which are precisely the ones we want to detect, are outliers with respect to the background and do not conform to the standard brain tissue templates. A robust estimation algorithm is thus needed to properly estimate the background without being affected by these outliers.

Our proposed spatial GMM fitting procedure extends the standard spatial GMM in two ways. First, we use the probability maps produced from the baseline scan (Scan 1) by the SPM software, but we update the probability maps to include both scans 1 and 2 as bivariate measurements. Our model thus extends the univariate model of Ashburner and Friston (2005) imple-

mented in SPM to multivariate cases, allowing multiple scans for the same subject. The usage of bivariate GMM adjusts the background of multiple scans simultaneously, considering correlations between scans from the same subject.

Furthermore, to estimate the mixture model parameters and probability maps, we propose a robust EM algorithm. The proposed algorithm uses a robust M -estimation step for updating the mean and covariance parameters, which is essential for the application since there are outliers such as tumor lesions present in the observation. The proposed robust EM algorithm is more objective and reliable than the estimation approaches in Guo et al. (2014) and Qin et al. (2017). In Guo et al. (2014), the background parameters were estimated from the data in manually selected healthy slices, but this was shown in Qin et al. (2017) to be unstable. Qin et al. (2017) used the entire brain volume but iterated the background estimation with the detection of outliers in an alternate fashion. Instead, our robust M -step is directly incorporated into the EM algorithm, and is based on statistical theory of robust estimation which is shown in our simulations to give remarkably accurate results. It is worth mentioning that another option for robust estimation may be to use a GMM with extra components for the outliers. However, a prior template map would not be available for the outliers because lesions do not occur at predictable spatial locations. Moreover, prior templates are obtained from healthy subjects who have no lesions present at all.

Both univariate and bivariate simulations are used to evaluate the tail probabilities after standardization of the Gaussian mixture when all the model parameters are estimated via the proposed robust EM algorithm. We show that the proposed robust EM algorithm is accurate without outliers but robust when outliers are present, and show that the obtained standardized scores from background adjustment methods with soft assignment have tail probabilities that are either very close to or more conservative than standard normal. In addition, we observe that background adjustment methods based on estimated parameters surprisingly have slightly better performances than the one with true parameters.

For brain images, the proposed approach can be applied directly by practitioners since the calculated scores and resulting p -values provide immediate reference for inferences about the change in disease status. We emphasize that although this paper is motivated by PET image analysis in oncology, the concepts of standardization of multivariate Gaussian mixtures and robust EM algorithm are generic, and can be used in other contexts. The Matlab toolbox **RB-SGMM-BA** is available online in Matlab Central to implement the proposed methods. Supplementary materials contain all proofs and

additional simulation studies.

2. Standardization of multivariate Gaussian mixtures. Let y be a random p -dimensional vector ($p \geq 1$) generated by a Gaussian mixture model (GMM) with K components:

$$(2.1) \quad f(y) = \sum_{k=1}^K \pi_k \phi(y|\mu_k, \Sigma_k),$$

where each $\pi_k > 0$ and $\sum_{k=1}^K \pi_k = 1$, and $\phi(\cdot; \mu_k, \Sigma_k)$ is the probability density function of a p -dimensional Gaussian variable with mean μ_k and covariance matrix Σ_k i.e. $N(\mu_k, \Sigma_k)$. Let the allocation variable $c \in \{1, 2, \dots, K\}$ mark the class from which y is generated, and let $s_k = \mathbb{1}(c = k)$, where $\mathbb{1}(\cdot)$ is the indicator function. Then we can represent the model (2.1) using the latent variables c 's as $P(c = k) = \pi_k$ and $y|c \sim N(\mu_c, \Sigma_c)$, or equivalently using the indicators s_k and $\mathbf{s} = \{s_1, \dots, s_K\}$:

$$(2.2) \quad \mathbf{s} \sim \text{Multinomial}(1; \pi_1, \dots, \pi_K), \quad y|\mathbf{s} \sim N\left(\sum_{k=1}^K s_k \mu_k, \sum_{k=1}^K s_k \Sigma_k\right).$$

2.1. Standardization methods. Let $\phi_k(\cdot) = \phi(\cdot|\mu_k, \Sigma_k)$. Then the posterior probability $w_k = P(c = k|y) = P(s_k = 1|y)$ that y belongs to the k th class is given by

$$(2.3) \quad w_k = \frac{\pi_k \phi_k(y)}{\sum_{k=1}^K \pi_k \phi_k(y)}$$

according to the Bayes' theorem. The posterior probability w_k is often referred to in the literature as the *membership weight* or *responsibility* of class k for y . The following two methods are commonly used in practice to recover the latent labels s_k 's:

- Hard assignment: assign $\tilde{s}_k = 1$ if $k = \arg \max_{k'} w_{ik'}$; otherwise, $\tilde{s}_k = 0$.
- Soft assignment: assign $\tilde{s}_k = w_k$.

Based on the membership weights, we wish to adjust the mean and covariance of each observation y with the hope that its resulting distribution will be close to a multivariate standard normal. To achieve this, consider the following representation of model (2.1). Let $Z \sim N(0, I_p)$, where I_p is the $p \times p$ identity matrix. Conditional on \mathbf{s} , the observation y is multivariate normal with mean $\sum_{k=1}^K s_k \mu_k$ and covariance $\sum_{k=1}^K s_k \Sigma_k$, which is identically

distributed as the random variable

$$(2.4) \quad Y = \left(\sum_{k=1}^K s_k \Sigma_k^{1/2} \right) Z + \sum_{k=1}^K s_k \mu_k,$$

where $\Sigma^{1/2}$ is the principal square root matrix of a positive definite matrix Σ such that $\Sigma^{1/2}$ is positive definite and $\Sigma^{1/2}\Sigma^{1/2} = \Sigma$. Since the s_k are 0-1 indicators, we can rewrite (2.4) as $Z = \left(\sum_{k=1}^K s_k \Sigma_k^{-1/2} \right) \left(y - \sum_{k=1}^K s_k \mu_k \right)$. If the latent labels s_k 's were known, this equation would provide an exact linear transformation to a multivariate standard normal distribution. Since the latent labels s_k 's are not known, we use the following plug-in transformation via the estimated labels \tilde{s}_k :

$$(2.5) \quad T^{(1)} = \left(\sum_{k=1}^K \tilde{s}_k \Sigma_k^{-1/2} \right) \left(y - \sum_{k=1}^K \tilde{s}_k \mu_k \right).$$

This will be our transformation of choice in Section 2.2 to Section 2.5. In the same spirit, one may also consider to calculate the combination of covariance matrices first and then invert, leading to the transformation

$$(2.6) \quad T^{(2)} = \left(\sum_{k=1}^K \tilde{s}_k \Sigma_k \right)^{-1/2} \left(y - \sum_{k=1}^K \tilde{s}_k \mu_k \right).$$

Other similar expressions are also possible. In particular, [Guo et al. \(2014\)](#) proposed to use the marginal covariance of Y , i.e.,

$$(2.7) \quad T^{(3)} = \tilde{\Sigma}^{-1/2}(y - \tilde{\mu}),$$

where $\tilde{\mu} = \sum_{k=1}^K \tilde{s}_k \mu_k$ and $\tilde{\Sigma} = \sum_{k=1}^K \tilde{s}_k [\Sigma_k + (\mu_k - \tilde{\mu})(\mu_k - \tilde{\mu})^T]$.

The three transformations (2.5), (2.6) and (2.7) yield exact multivariate standard normal if the latent labels \tilde{s}_k are replaced by the true values s_k . They are equivalent if hard assignment is used in the estimation of latent labels, but not so if soft assignment is used. For this reason, whenever we need to distinguish between soft and hard assignment in what follows, we use the generic notations $T_S^{(1)}$, $T_S^{(2)}$ and $T_S^{(3)}$ respectively for the three transformations with the soft assignment, and use T_H for the transformation with the hard assignment.

The goal of the rest of this section is to determine parameter scenarios under which the distributions of the standardized scores $T^{(1)}$, $T^{(2)}$ and $T^{(3)}$ are close to multivariate standard normal. We focus on the transformation

$T^{(1)}$ because it is the easiest to analyze theoretically. This is sufficient because, as we shall see later in the simulations, the other two transformations $T^{(2)}$ and $T^{(3)}$ perform similarly.

Throughout this section, we consider the situation $K = 2$ for simplicity, although the same ideas apply to a higher number of classes.

2.2. Reparametrization of the standardized scores. When $K = 2$, the standardized score $T^{(1)}$ in equation (2.5) can be written as

$$\begin{aligned} T^{(1)} &= (\tilde{s}_1 \Sigma_1^{-1/2} + \tilde{s}_2 \Sigma_2^{-1/2})(Y - \tilde{s}_1 \mu_1 - \tilde{s}_2 \mu_2) \\ &= \begin{cases} (\tilde{s}_1 I + \tilde{s}_2 \tau)(Z + \tilde{s}_2 \Delta_1) & s_1 = 1; \\ (\tilde{s}_1 \tau^{-1} + \tilde{s}_2 I)(Z - \tilde{s}_1 \tau \Delta_1) & s_1 = 0, \end{cases} \end{aligned}$$

where $\Delta_1 = \Sigma_1^{-1/2}(\mu_1 - \mu_2)$ and $\tau = \Sigma_2^{-1/2}\Sigma_1^{1/2}$. Let the ratio between likelihoods of the two components be $r(y) = 2 \log(\phi_1(y)/\phi_2(y))$ and let $\pi_0 = 2 \log(\pi_2/\pi_1)$. Then the posterior probabilities in (2.3) become

$$(2.8) \quad w_1 = \frac{1}{1 + \exp(-\frac{1}{2}(r(Y) - \pi_0))}; \quad w_2 = \frac{1}{1 + \exp(\frac{1}{2}(r(Y) - \pi_0))}.$$

Noting that $|\tau| = |\Sigma_2|^{-1/2}|\Sigma_1|^{1/2}$, i.e. $\log |\tau| = -(\log |\Sigma_2| - \log |\Sigma_1|)/2$, we have that

$$r(Y) = -2 \log |\tau| + \begin{cases} (\tau Z + \tau \Delta_1)^T (\tau Z + \tau \Delta_1) - Z^T Z & s_1 = 1; \\ Z^T Z - (\tau^{-1} Z - \Delta_1)^T (\tau^{-1} Z - \Delta_1) & s_1 = 0, \end{cases}$$

or equivalently,

$$\begin{aligned} r(Y) &= -2 \log |\tau| + [(\tau Z + \tau \Delta_1)^T (\tau Z + \tau \Delta_1) - Z^T Z] \cdot \mathbb{1}(s_1 = 1) \\ &\quad + [Z^T Z - (\tau^{-1} Z - \Delta_1)^T (\tau^{-1} Z - \Delta_1)] \cdot \mathbb{1}(s_1 = 0). \end{aligned}$$

For hard assignment, $\tilde{s}_1 = \mathbb{1}(r(Y) > \pi_0) = \mathbb{1}(w_1 > 1/2)$ according to equation (2.8), and $\tilde{s}_2 = 1 - \tilde{s}_1$. We thus can represent T_H as follows: $T_H = Z$ if $s_1 = \tilde{s}_1$; $T_H = \tau^{-1} Z - \Delta_1$ if $\tilde{s}_1 = 1, s_1 = 0$; and $T_H = \tau Z + \tau \Delta_1$ if $\tilde{s}_1 = 0, s_1 = 1$, i.e.

$$T_H = Z \cdot \mathbb{1}(\tilde{s}_1 = s_1) + (\tau^{-1} Z - \Delta_1) \cdot \mathbb{1}(\tilde{s}_1 > s_1) + (\tau Z + \tau \Delta_1) \cdot \mathbb{1}(\tilde{s}_1 < s_1).$$

In contrast, the soft assignment estimates the labels according to the posterior probabilities, i.e. $\tilde{s}_1 = w_1$ and $\tilde{s}_2 = w_2$.

The full model depends on the parameter space $\Theta = \{(\mu_1, \mu_2, \Sigma_1, \Sigma_2, \pi_1, \pi_2) : \mu_1, \mu_2 \in \mathbb{R}^p, \Sigma_1, \Sigma_2 \in \mathbb{R}^{p \times p}, \pi_1, \pi_2 \in [0, 1], \pi_1 + \pi_2 = 1\}$ of dimension

$2p + 2p(p+1)/2 + 1 = p^2 + 3p + 1$. However, the transformation $T^{(1)}$ in (2.5) only depends on the full parameter space through a lower dimensional subset (Δ_1, τ, π_0) of dimension $p + p(p+1)/2 + 1 = (p^2 + 3p + 2)/2$. This appealing property does not generally hold for the other two transformations $T^{(2)}$ and $T^{(3)}$ in (2.6) and (2.7). For example, since Σ_1 and Σ_2 are not always simultaneously diagonalizable, the term $(\tilde{s}_1 \Sigma_1 + \tilde{s}_2 \Sigma_2)^{-1/2}$ in the transformation $T_S^{(2)}$ cannot decompose into the simpler form as it is for $T^{(1)}$.

2.3. Approximate normality. While our goal is to compare the tail probabilities between the standardized score $T^{(1)}$ and a standard multivariate normal Z , it can be seen that the former approximates the latter over the entire domain under several extreme parameter scenarios.

Let $\Theta_0 = \{\mu_1 = \mu_2, \Sigma_1 = \Sigma_2\} \cup \{\pi_1 = 1 \text{ or } \pi_2 = 1\} = \{\Delta_1 = 0, \tau = I_p\} \cup \{|\pi_0| = +\infty\}$. The set Θ_0 trivially leads to perfect standardization so that $T^{(1)} = Z$, as the mixture model becomes one single component. This holds for any values of the parameters inside Θ_0 , so identifiability is not important in this case. The following theorem states that approximate normality also holds when the parameters are either close to or far from the set Θ_0 . Let $\|\cdot\|_2$ denote the Euclidean norm in the case of a vector or the Frobenius norm in the case of a matrix.

THEOREM 2.1. *For both hard and soft assignments, if $(\Delta_1, \tau, \pi_0) \in \Theta_0^c$ are bounded, then we have the following results:*

- 1) *For fixed (Δ_1, τ) , assume there is a sequence of parameters (π_1, π_2) such that $\pi_1 \rightarrow 1$ or $\pi_2 \rightarrow 1$, then $T^{(1)} \xrightarrow{p} Z$.*
- 2) *For fixed (π_1, π_2) , assume that there is a sequence of parameters (Δ_1, τ) such as $\|\Delta_1\|_2 \rightarrow +\infty$ and $\|\tau\|_2$ is bounded, then $T^{(1)} \xrightarrow{a.s.} Z$.*
- 3) *If there is a sequence of parameters (Δ_1, τ) such as $\|\Delta_1\|_2 \rightarrow 0$ and $\|\tau - I_2\|_2 \rightarrow 0$, then $T^{(1)} \xrightarrow{a.s.} Z$.*
- 4) *If there is a sequence of parameters (Δ_1, τ) and a vector a such as $a^T \Delta_1 \rightarrow 0$ and $\|\tau - A\|_2 \rightarrow 0$ where $Aa = a$, then $a^T T^{(1)} \xrightarrow{a.s.} a^T Z$.*

REMARK 2.2. In Theorem 2.1 (1), we can obtain a.s. convergence for $T^{(1)}$ if π_1 goes to 0 or 1 fast, for instance, if $\sum_n \pi_1^{(n)} \wedge \pi_2^{(n)} < \infty$ by the Borel-Cantelli lemma.

Theorem 2.1 states that the standardized score will be approximately standard multivariate normal (with convergence in probability or almost surely) if one of the following occurs in a limiting sense: (1) one of the mixture components is dominant; (2) the mean vectors of the two components are well separated relative to the covariance matrices; (3) the mean vectors and

covariance matrices of the two components are close to each other; (4) the mean vectors and covariance matrices of the two components are close to each other along a particular direction, in which case normality is obtained on the corresponding contrast along that direction.

REMARK 2.3. Items (1), (2) and (4) in Theorem 2.1 discusses $\theta \in \Theta_0^c$ and describe scenarios where $\theta \rightarrow \theta_0$ for some $\theta_0 \in \Theta_0$. Therefore, the results in Theorem 2.1 ensure that the standardized score $T^{(1)}$ is continuous at Θ_0 .

REMARK 2.4. Note that it is a special case when the two covariance matrices are the same, i.e. $\tau = I_p$. In this case, we have $\Delta_1 = \Delta_2$ and the results in Theorem 2.1 still hold.

2.4. *Explicit distribution in the case of hard assignment.* To further understand the behavior of the standardized scores in scenarios other than those considered in Theorem 2.1, it is helpful to have an explicit formula for the distribution of $T^{(1)}$. This is also useful in the numerical evaluations in Section 2.5 below.

Let $F_X(\cdot)$ denote the CDF of a random variable X , $\Phi(\cdot)$ be the CDF of standard normal and $\Phi_p(\cdot)$ be the distribution function of a p -dimensional standard normal Z , i.e., $\Phi_p(A) = P(Z \in A)$ for a Borel set A . Then Theorem 2.5 gives the exact CDF of a contrast on T_H .

THEOREM 2.5. Define the two maps g and h as $g : \mathbb{R}^p \rightarrow \mathbb{R}^p, g(x) = \tau x + \tau \Delta_1$ and $h : \mathbb{R}^p \rightarrow \mathbb{R}^p, h(x) = -x^T x + (\tau x + \tau \Delta_1)^T (\tau x + \tau \Delta_1) - 2 \log |\tau|$. For a given vector $a \in \mathbb{R}^p$ such that $\|a\|_2 = 1$ and any $t \in \mathbb{R}$, we have

$$F_{a^T T_H}(t) - \Phi(t) = \pi_1 [\Phi_p(g^{-1}(R_2) \cap R_3) - \Phi_p(R_2 \cap R_3)] \\ + \pi_2 [\Phi_p(g(R_2) \cap g(R_3^c)) - \Phi_p(R_2 \cap g(R_3^c))],$$

where $R_2 = \{x : a^T x < t\}$, $R_3 = \{x : h(x) < \pi_0\}$ and g^{-1} is the inverse map of g .

The set R_3 in Theorem 2.5 involves the quadratic form $h(x)$ in x if $\tau \neq I_p$. When $p = 1$, we actually can solve this quadratic equation $h(x) = \pi_0$ explicitly as follows. Without loss of generality, we consider the case when $\tau \geq 1$.

LEMMA 2.6. Assume that the dimension $p = 1$, $\theta \in \Theta_0^c$ and $\tau \geq 1$. Let $c_0 = (\tau^2 - 1)(\pi_0 + 2 \log \tau) + \Delta_2^2$ and $c_0^+ = \max(c_0, 0)$. Then the set

$R_3 = \{h(x) < \pi_0\} = (a_-(\theta), a_+(\theta))$, where

$$\begin{aligned}
 (2.9a) \quad & \left(\frac{-\tau\Delta_2 - \sqrt{c_0^+}}{\tau^2 - 1}, \frac{-\tau\Delta_2 + \sqrt{c_0^+}}{\tau^2 - 1} \right) \quad \text{if } \tau > 1 \\
 (2.9b) \quad & (a_-(\theta), a_+(\theta)) = \begin{cases} \left(-\infty, \frac{\pi_0}{2\Delta_2} - \frac{\Delta_2}{2} \right) & \text{if } \tau = 1 \text{ and } \Delta_2 > 0 \\ \left(\frac{\pi_0}{2\Delta_2} - \frac{\Delta_2}{2}, +\infty \right) & \text{if } \tau = 1 \text{ and } \Delta_2 < 0. \end{cases} \\
 (2.9c) \quad &
 \end{aligned}$$

REMARK 2.7. The situation when $\tau = 1$ means that the two variances are the same. The definitions of $a_{\pm}(\theta)$ in (2.9b) and (2.9c) can actually be obtained by applying L'Hospital's Rule to the expressions in (2.9a) when $\tau \rightarrow 1+$ (limit from above). This suggests a continuous behavior of the set R_3 when the variances of different components change from the heterogeneous to homogeneous.

For simplicity of notation, we now drop the argument θ when referring to $a_-(\theta), a_+(\theta)$. The following Theorem 2.8 gives the explicit formula for the CDF of T_H , which is obtained by combining Theorem 2.5 and Lemma 2.6.

THEOREM 2.8. Assume that the dimension $p = 1$, $\theta \in \Theta_0^c$ and $\tau \geq 1$. We have

$$\begin{aligned}
 F_{T_H}(t) = & \Phi(t) + \pi_1[\Phi((b_- \vee (t \wedge b_+))/\tau - \Delta_1) - \Phi(a_- \vee (t \wedge a_+))] \\
 & + \pi_2[\Phi(\tau(t \wedge a_-) + \Delta_2) + \Phi(\tau(t \vee a_+) + \Delta_2) - \Phi(t \wedge b_-) - \Phi(t \vee b_+)],
 \end{aligned}$$

for any $t \in \mathbb{R}$, where $b_- = \tau a_- + \Delta_2$, $b_+ = \tau a_+ + \Delta_2$, and the operator \wedge and \vee are the min and max operator, i.e. for any $a, a' \in \mathbb{R}$, $a \wedge a' = \min(a, a')$, and $a \vee a' = \max(a, a')$.

2.5. *Numerical evaluation of tail probabilities.* From Theorem 2.1 we learn that the scenarios in which the standardized score may be far from standard multivariate normal are those where the mixture components are not close to each other nor far from each other. In this section, we study some of these scenarios numerically. We focus on tail probabilities, which are most important for statistical testing.

Let the vector a be the contrast of interest and let α be the size of the test. If the decision threshold is set as $t_\alpha = \Phi^{-1}(\alpha/2)$, according to the standard normal distribution, then we are interested in whether the true size of the test is below or above α . The true size of a two-sided hypothesis test is

$P(|a^T T^{(1)}| \geq t_\alpha) = F_{a^T T}(t_\alpha) + 1 - F_{a^T T}(-t_\alpha)$. Let $R(\alpha) = P(|a^T T^{(1)}| \geq t_\alpha)/\alpha$ be the ratio between the true size of the test and the size based on the standard normal distribution: $R(\alpha) = 1$ means that the size is exact; $R(\alpha) < 1$ means that the test is conservative; $R(\alpha) > 1$ means that the test is invalid.

In this section we study the relative size $R(\alpha)$ for various combinations of model parameters (Δ_1, τ, π_0) . We may also write $R(\alpha; \Delta_1, \tau, \pi_0)$ to emphasize the dependence of this ratio on the parameters (Δ_1, τ, π_0) . As a reduction on the set of parameters to be evaluated, the following Lemma 2.9 states that the relative size $R(\alpha; \Delta_1, \tau, \pi_0)$ is symmetric with respect to the sign of Δ_1 ; thus changes in Δ_1 need only be evaluated in one direction.

LEMMA 2.9. *For any $t \in \mathbb{R}$, we have*

$$P(|a^T T^{(1)}| \geq t; \Delta_1, \tau, \pi_0) = P(|a^T T^{(1)}| \geq t; -\Delta_1, \tau, \pi_0).$$

A theoretical expression for $R(\alpha)$ for soft assignment is difficult to obtain. Instead, we use numerical evaluation to investigate the tail probabilities via Monte Carlo simulation. For simplicity, we focus on the bivariate case $p = 2$. Similar to the data analysis, we use $a^T = (1, -1)/\sqrt{2}$ as the contrast of interest, measuring the normalized difference between the two coordinates of $T^{(1)}$. Since the distribution of $a^T T^{(1)}$ depends only on the parameters (Δ_1, τ, π_0) , we assume without loss of generality $\mu_2 = 0$ and $\Sigma_2 = I$ when generating the data Y . We use the following parameter settings to investigate the tail probabilities:

$$\begin{aligned} \text{Case 1: } \quad & \mu_1 = \kappa_1 \begin{pmatrix} 1 \\ 1 \end{pmatrix}, \quad \Sigma_1 = \kappa_2 \begin{pmatrix} 1 & \rho \\ \rho & 1 \end{pmatrix}; \quad \mu_2 = 0, \quad \Sigma_2 = I. \\ \text{Case 2: } \quad & \mu_1 = \kappa_1 \begin{pmatrix} 2/\sqrt{5} \\ 1/\sqrt{5} \end{pmatrix}, \quad \Sigma_1 = \kappa_2 \begin{pmatrix} 1 & \rho \\ \rho & 1 \end{pmatrix}; \quad \mu_2 = 0, \quad \Sigma_2 = I. \end{aligned}$$

In the above setting, the parameter ρ controls the correlation of the bivariate normal in the first class, while κ_1 and κ_2 control how the two classes differ from each other.

Figure 3 illustrate schematically the density contours of the two cases when $\rho = 0.5$. In Case 1, the vector Δ_1 is orthogonal to the contrast vector a , while in Case 2 it is not.

Figures 4 and 5 below show the relative size $R(\alpha)$ for $\alpha = 0.001$ in the form of heatmaps when $\rho \in \{0, 0.5\}$, $\kappa_2 = (0.1, 1, 10)$ and κ_1 and π_1 vary continuously. Note that because of Lemma 2.9, it is sufficient to consider $\kappa_1 \geq 0$. In these figures, purple is ideal, indicating a relative size of about 1. Blue indicates a conservative relative size smaller than 1, while red indicates

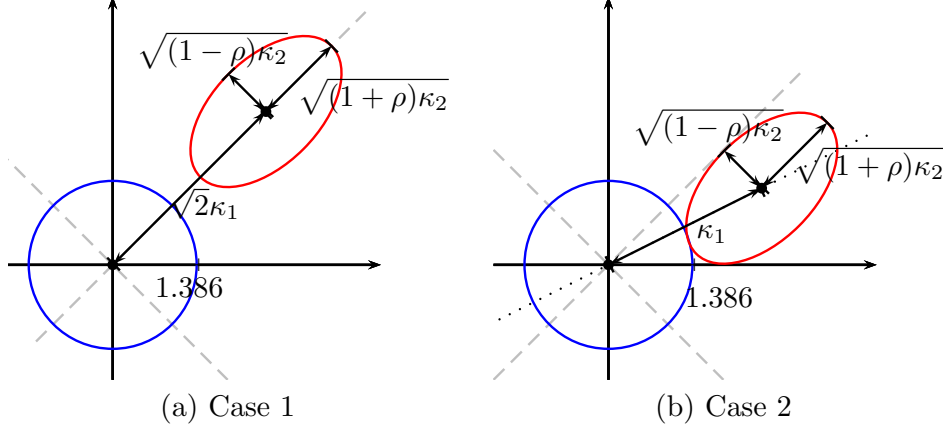


Fig 3: 50% density contours of the two bivariate mixture components used for numerical evaluation of tail probabilities of the standardized score when $\rho = 0.5$. The red ellipse represents the density contour of the first class, while the blue circle centered at the origin represents the density contour of the second class. The two plots use $\kappa_2 = 1.923$ (both cases), $\kappa_1 = 2.773$ (Case 1) and $\kappa_1 = 3.100$ (Case 2) for demonstration.

an invalid relative size greater than 1. Black indicates a relative size greater than 2, which may be considered unacceptable.

To see how these parameter combinations fall into the parameter settings in Theorem 2.1, we compute

$$\tau = \Sigma_2^{-1/2} \Sigma_1^{1/2} = \frac{\sqrt{\kappa_2}}{2} \begin{pmatrix} \sqrt{1+\rho} + \sqrt{1-\rho} & \sqrt{1+\rho} - \sqrt{1-\rho} \\ \sqrt{1+\rho} - \sqrt{1-\rho} & \sqrt{1+\rho} + \sqrt{1-\rho} \end{pmatrix}$$

and $\Delta_1 = \Sigma_1^{-1/2}(\mu_1 - \mu_2)$ as:

$$\text{Case 1: } \Delta_1 = \Sigma_1^{-1/2}(\mu_1 - \mu_2) = \frac{\kappa_1}{\sqrt{\kappa_2}(1-\rho)} \begin{pmatrix} 1 \\ 1 \end{pmatrix}$$

$$\text{Case 2: } \Delta_1 = \frac{\kappa_1}{2\sqrt{5\kappa_2}} \begin{pmatrix} -1/\sqrt{1-\rho} + 3/\sqrt{1+\rho} \\ 1/\sqrt{1-\rho} + 3/\sqrt{1+\rho} \end{pmatrix}.$$

As predicted by Theorem 2.1, the relative sizes are all close to 1 for extreme values of π_1 close to 0 or 1 in all subplots (satisfying conditions in Theorem 2.1 (1)), large κ_1 with respect to κ_2 (satisfying conditions in (2) as $\|\Delta_1\|_2$ is large), and $\kappa_2 = 1$ and $\rho = 0$ (satisfying conditions in (4) as $\tau = I_2$ and $a^T \Delta_1 = 0$).

When comparing hard and soft assignment, Figure 4 shows that, in Case 1, hard assignment leads to unacceptable relative sizes regardless of the mixture proportion π_1 , especially when κ_1 is small. Soft assignment, however, corrects this and leads to conservative relative sizes in all the cases shown. A similar pattern is observed in Figure 5 for Case 2, except that soft assignment leads to relative sizes slightly greater than 1 for some parameter combinations. More combination of parameters studied, including evaluation of one-sided tail probabilities, lead to similar observations and thus are not included due to space limitations.

3. Spatial and robust fitting of Gaussian mixture models. To fit the PET data as a Gaussian mixture model requires two particular features. One is to incorporate a spatial component into the model, so that the prior probabilities vary according to a spatial pattern defined by the tissue types. These spatial patterns can be incorporated into the EM algorithm via pre-defined spatial templates. The second feature is to make the M step in the EM algorithm robust to outliers so that estimation of the background is not affected by tumor voxels. The tumor voxels cannot be modeled as a separate component in the mixture such as in because they are relatively few in volume and because they do not correspond to any particular spatial pattern known a-priori.

3.1. Spatial Gaussian mixture models. Most existing approaches about spatial GMM are based on the Markov random field on π_{ik} such as the method of iterated conditional modes in (Besag, 1986), discussions in Chapter 13 of McLachlan and Peel (2000), and many other developments along this line (Sanjay-Gopal and Hebert, 1998a; Thanh Minh Nguyen and Wu, 2012; Vehtari and Ojanen, 2012). However, in our applications template maps of the class membership probability are available from brain atlases (Ashburner, 2012), which makes it more sensible to adopt an approach that utilizes the existing spatial templates.

Let the observations be $\{y_i\}_{i=1}^n$, where y_i is a p -dimensional vector ($p \geq 1$) at the i th location and n is the total number of voxels. For 2-dimensional or higher dimensional images where the location index has more than one direction, we can vectorize the location to have this single index i . We assume that the y_i 's are independently generated by a GMM in (2.1) but with a spatial mixture probabilities:

$$(3.1) \quad f(y_i) = \sum_{k=1}^K \pi_{ik} \phi(y_i | \mu_k, \Sigma_k),$$

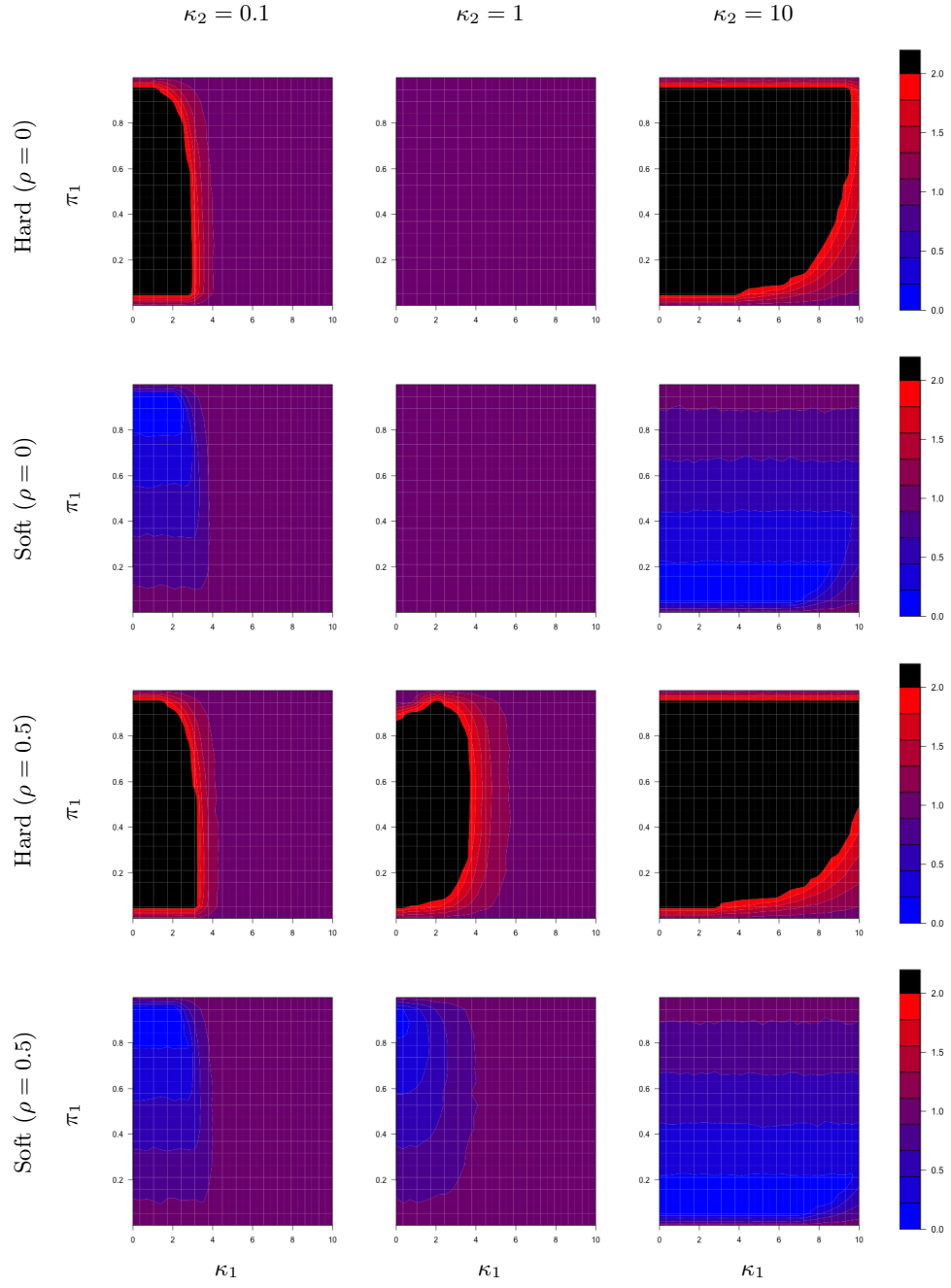
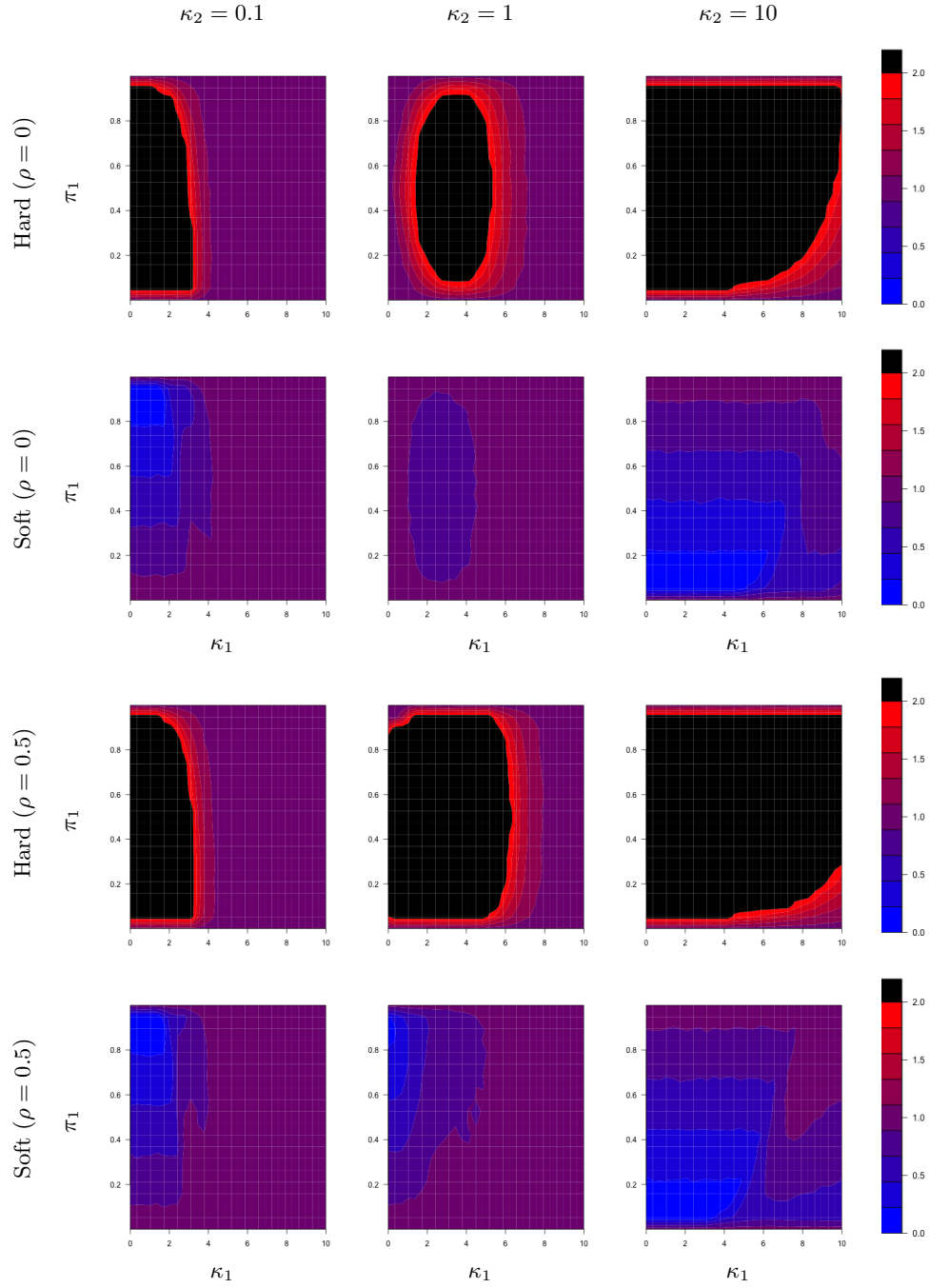


Fig 4: Heatmaps of $R(\alpha)$ (two-side tails) where $\alpha = 0.001$ for Case 1.

Fig 5: Heatmaps of $R(\alpha)$ (two-side tails) where $\alpha = 0.001$ for Case 2.

where $\sum_{k=1}^K \pi_{ik} = 1$ for any i and $\pi_{ik} > 0$. We refer to model (3.1) as a Spatial Gaussian Mixture Model (SGMM).

The traditional Gaussian Mixture Model (GMM) assumes that $\pi_{ik} = \pi_k$ for all i . In contrast, SGMM considers the spatial information by using different mixture probabilities at each location. In order to incorporate spatial information, we assume that the probability maps are generated by some given prior probability maps b_{ik} :

$$(3.2) \quad \pi_{ik} = \gamma_k b_{ik} \left\{ \sum_{j=1}^K \gamma_j b_{ij} \right\}^{-1},$$

with the identifiability constraint $\sum_{k=1}^K \gamma_k = 1$, which is also used by [Ashburner and Friston \(2005\)](#). The probability maps b_{ik} are often referred to as templates. Spatial templates provide a natural way to incorporate prior knowledge from previous studies about the probability of each location i belonging to each class. In the case of the brain, the templates represent reference probability maps for brain tissue types like GM, WM and CSF. Such templates, constructed from segmentations of images of healthy subjects, are available within the software SPM. Other ways to introduce the probability map π_{ik} are possible but may have more parameters to estimate, such as the one based on Markov random field ([Sanjay-Gopal and Hebert, 1998b](#); [Chen et al., 2001](#); [Soffientini et al., 2016](#))

The usage of templates also reduces the dimension of the parameters in the model, which otherwise would be nearly proportional to the number of voxels n . Under the constraint (3.2), the parameters of model (2.2) become $\theta = (\mu_k, \sigma_k, \gamma_k)_{k=1}^K$, with dimension $K[p + p(p+1)/2] + (K-1)$. For $p = 2$ and $K = 3$, the dimension is 17. It can be seen again that the traditional GMM is a special case of SGMM by letting $b_{ik} = b_k$ for all i in (3.2), i.e. the traditional GMM uses constant template maps.

Given all parameters, the standardized scores at each location i can be obtained using the methods introduced in Section 2. In Section 3.2, we propose a robust expectation-maximization (EM) algorithm to obtain maximum likelihood estimators (MLE) in model (3.1). The tail probabilities and performances of the robust EM algorithm are investigated through simulation in Section 4.

3.2. Robust EM algorithm. The EM algorithm introduced by [Dempster et al. \(1977\)](#) and its invariants are popular to obtain the maximum likelihood estimators (MLE) in a mixture model; see [McLachlan and Krishnan \(2008\)](#) for a comprehensive treatment. Since the model of SGMM (2.1)

uses spatial mixture probabilities via the parameterization (3.2), the conventional EM does not apply directly and modifications are needed to make the EM algorithm work, which results in a generalized EM algorithm. Furthermore, voxels that exhibit large changes in intensity such as lesions, which are precisely the ones we want to detect, are outliers with respect to the background. A robust estimation procedure is thus necessary to properly estimate the background without being affected by these outliers. As robust estimators, M -estimators in mixture models have been well developed in the literature (Campbell, 1984; McLachlan and Basford, 1988; Maronna et al., 2006). The basic idea is to reduce the weights of abnormal observations while keeping close to full weights for the others. We shall use M -estimates in the M -step of an EM algorithm to achieve robust fitting of SGMM.

Let $\mathbf{y} = (y_1, \dots, y_n)$, then the log-likelihood function is given by

$$(3.3) \quad \ell(\theta; \mathbf{y}) = \sum_{i=1}^n \log \left\{ \sum_{k=1}^K \pi_{ik} \phi_k(y_i | \mu_k, \Sigma_k) \right\}.$$

If the latent labels $\mathbf{s} = (s_{11}, \dots, s_{1K}; \dots; s_{n1}, \dots, s_{nK})$ are observed, the joint log-likelihood is

$$(3.4) \quad \ell(\theta; \mathbf{y}, \mathbf{s}) = \sum_{i=1}^n \sum_{k=1}^K s_{ik} [\log(\pi_{ik}) + \log(\phi(y_i | \mu_k, \Sigma_k))].$$

Given an intermediate estimate θ^t , we first calculate the conditional expectation of $\ell(\theta; \mathbf{y}, \mathbf{s})$ in equation (3.4) denoted as $Q(\theta | \theta^t)$ (the E-step), and then maximize this conditional expectation with robustness (the robust M-step). For the robustness step, we use the Mahalanobis distance between observations and the estimated mean vectors and covariance matrices to determine whether an observation is abnormal or not. Given the distance, observations are weighted according to the weight function $u(s) = \psi(s)/s$ where $\psi(s) = \min(s, k_1(p))$ is Huber's ψ -function (Huber, 1964; Maronna, 1976) with a tuning constant $k_1(p)$ depending on the dimension p . We next present the detailed generalized EM algorithm.

- E-step. Conditional Expectation on \mathbf{y}, θ^t :

$$\begin{aligned} Q(\theta | \theta^t) &= \sum_{i=1}^n \sum_{k=1}^K E(s_{ik} | \mathbf{y}, \theta^t) [\log(\pi_{ik}) + \log(\phi(y_i | \mu_k, \Sigma_k))] \\ &= \sum_{i=1}^n \sum_{k=1}^K w_{ik}^t [\log(\pi_{ik}) + \log(\phi(y_i | \mu_k, \Sigma_k))], \end{aligned}$$

where

$$w_{ik}^t = E(s_{ik}|\mathbf{y}, \theta^t) = \frac{\pi_{ik}^t \phi(y_i|\mu_k^t, \Sigma_k^t)}{\sum_{k=1}^K \pi_{ik}^t \phi(y_i|\mu_k^t, \Sigma_k^t)}, \quad \text{and} \quad \pi_{ik}^t = \frac{\gamma_k^t b_{ik}}{\sum_{k=1}^K \gamma_k^t b_{ik}}.$$

- Update γ_k :

$$(3.5) \quad \gamma_k^{t+1} = \sum_{i=1}^n \left\{ w_{ik}^t \left(\sum_{i=1}^n \frac{b_{ik}}{\sum_{j=1}^K \gamma_j^t b_{ij}} \right)^{-1} \right\}.$$

- Robust M-step.

Update the mean vector:

$$r_{ik}^{t,1} = \sqrt{(y_i - \mu_k^t)^T \Sigma_k^{-1} (y_i - \mu_k^t)}; \quad \mu_k^{t+1} = \frac{\sum_{i=1}^n w_{ik}^t u(r_{ik}^{t,1}) y_i}{\sum_{i=1}^n w_{ik}^t u(r_{ik}^{t,1})}.$$

Update the covariance matrix:

$$r_{ik}^{t,2} = \sqrt{(y_i - \mu_k^{t+1})^T \Sigma_k^{-1} (y_i - \mu_k^{t+1})};$$

$$\Sigma_k^{t+1} = \frac{\sum_{i=1}^n w_{ik}^t u^2(r_{ik}^{t,2}) (y_i - \mu_k^{t+1})(y_i - \mu_k^{t+1})^T}{\sum_{i=1}^n w_{ik}^t u^2(r_{ik}^{t,2})}.$$

The algorithm is terminated when the relative change of the log-likelihood function in (3.3) with respect to the previous iteration becomes smaller than a given tolerance or a maximum number of iterations is reached. The tuning parameter $k_1(p)$ in the robust M-step depends on the proportion of contaminated data in the observation. We use $k_1(p) = \sqrt{\chi_{p,\alpha}^2}$ where $\chi_{p,q}^2$ is the q th quantile of the χ_p^2 distribution as used in Devlin et al. (1981). In the provided toolbox **RB-SGMM-BA**, the default values for the tolerance, maximum number of iterations and q are $(10^{-5}, 1000, 0.99)$, respectively.

REMARK 3.1 (Comparison with the the conventional EM). The EM algorithm in the conventional GMM without spatial templates uses $\pi_{ik}^t = \pi_k^t$ and $\pi_k^t = \sum_{i=1}^n w_{ik}^t/n$ in the E-step and does not update γ_k . The M-step without robustness may update the mean vector and covariance matrix by

$$\mu_k^{t+1} = \frac{\sum_{i=1}^n w_{ik}^t y_i}{\sum_{i=1}^n w_{ik}^t}, \quad \Sigma_k^{t+1} = \frac{1}{\sum_{i=1}^n w_{ik}^t} \sum_{i=1}^n w_{ik}^t (y_i - \mu_k^{t+1})(y_i - \mu_k^{t+1})^T,$$

which can be viewed as a special case of the proposed robust EM algorithm where the weight function $u(s) = 1$ for all s .

REMARK 3.2 (Derivation of the robust EM algorithm). We just need to derive the update of γ_k as the E-step follows the conventional EM but has voxel-varying π_{ik} and π_{ik}^t , and the M-step is an application of M -estimation. The update of γ_k is obtained by solving $\partial Q(\theta|\theta^t)/\partial\gamma_k = 0$. Specifically,

$$\begin{aligned} Q(\theta|\theta^t) &= \sum_{i=1}^n \sum_{k=1}^K w_{ik}^t \log(\pi_{ik}) + \text{constant} \\ &= \sum_{i=1}^n \sum_{k=1}^K w_{ik}^t \log(\gamma_k b_{ik}) - \sum_{i=1}^n \sum_{k=1}^K w_{ik} \log \left(\sum_{j=1}^K \gamma_j b_{ij} \right) + \text{constant} \\ &= \sum_{i=1}^n w_{ik}^t \log(\gamma_k) - \sum_{i=1}^n \log \left(\sum_{j=1}^K \gamma_j b_{ij} \right) + \text{constant}, \end{aligned}$$

where the term *constant* is with respect to γ_k . Therefore, we obtain that

$$\frac{\partial Q(\theta|\theta^t)}{\partial\gamma_k} = \frac{\sum_{i=1}^n w_{ik}^t}{\gamma_k} - \sum_{i=1}^n \frac{b_{ik}}{\sum_{j=1}^K \gamma_j b_{ij}},$$

which is a nonlinear function of γ_k 's. Formula (3.5) is thus obtained if we calculate the term $\sum_{j=1}^K \gamma_j b_{ij}$ using γ_k^t in the previous iteration. This simplification leads to a generalized EM and has been observed to ensure convergence by [Ashburner and Friston \(2005\)](#).

It is worth mentioning that other robust estimation of mixture models may be also applicable, such as mixtures of heavy-tailed distributions such as t distributions in [\(McLachlan and Peel, 2000\)](#) or maximizing a transformed likelihood tailored for robustness [\(Qin and Priebe, 2013\)](#). Supplementary Materials contain a simulation study to compare the proposed robust EM algorithm with a mixture of t distributions in a non-spatial setting. The incorporation of the spatial structures implies non-trivial generalizations of these methods which we view as future research topics.

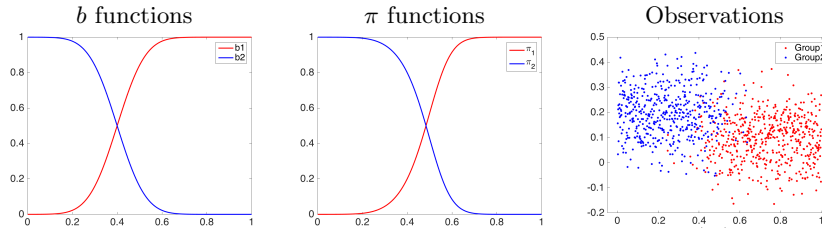
4. Simulation. Section 2 investigated the tail probabilities of $T^{(1)}$ when all parameters are given, a situation that we refer to as the “oracle”. In this section, we investigate the tail probabilities of $T^{(1)}$ when all the parameters are estimated via the proposed robust EM algorithm in Section 3.2.

4.1. Univariate Data. Although the real motivating data is bivariate, investigation of the univariate case is helpful because it is easier to interpret and provides insight for multivariate cases. Moreover, even for multivariate

data, the final quantity of interest is univariate when considering a contrast among the multivariate observations.

We simulate data according to model (2.1) and (3.2) with dimension $p = 1$. We use $K = 2$ classes and $n = 1000$ locations, where the parameters in the model are given by $b_1(t) = \Phi(10t - 4)$, $b_2(t) = 1 - b_1(t)$, $\gamma = (0.2, 0.8)$, $\mu = (0.1, 0.2)$, and $\sigma = (0.1, 0.1)$. Figure 6 shows the b and π functions, along with one simulated instance of the observations. Except for the right and left extremes where π_1 and π_2 are close to 0 or 1, the other parameter combinations do not correspond to the favorable parameter combinations of Theorem 2.1.

Fig 6: Simulation settings for the univariate case. The three plots are the template maps, transformed template maps and observations. The x -axis in each plot is the location t .



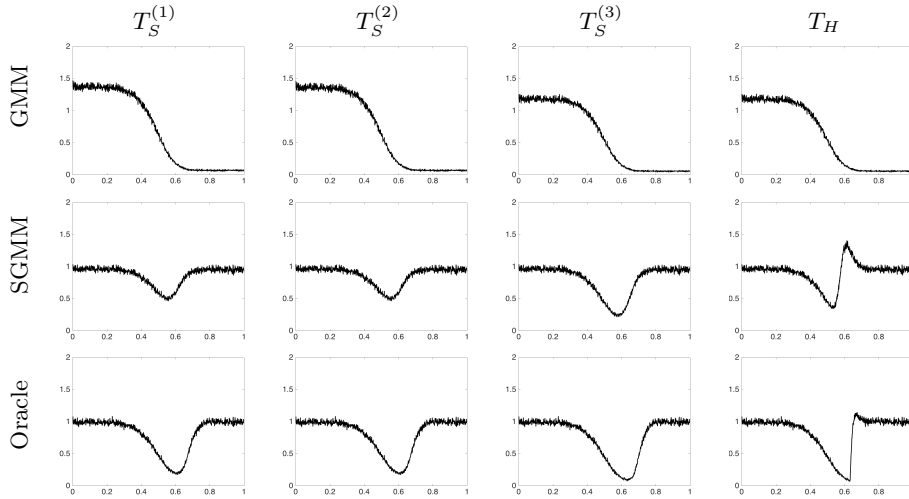
To estimate the model parameters, we apply the traditional GMM and the proposed Spatial GMM (without robust adjustments for now). The results are compared to those using the true parameters, referred to as “oracle”. To standardize the observations, we use both soft and hard assignments $T_S^{(1)}, T_S^{(2)}, T_S^{(3)}$ and T_H . We compare the methods by calculating the relative size $R(\alpha)$ for $\alpha = 0.01$, based on 10^5 simulations.

Figure 7 plots the relative size $R(0.01)$ for the right tail. We can see that the traditional GMM method leads to relative sizes both greater and smaller than 1 in different locations. The traditional GMM is heavily affected by the spatial structure of the π functions because it does not consider any spatial information in the probability templates. In contrast, the proposed SGMM with soft assignments lead to tail probabilities that are very close to standard normal, except in the middle locations where there is a strong mixing between the components and the relative size is conservative.

Furthermore, when the SGMM is used, soft assignment has better performance than hard assignment in the sense that the hard assignment leads to invalid relative sizes, while soft assignment does not. We can also see

that the oracle method using the true parameter values offers limited benefit with respect to SGMM with soft assignment, with the latter performing, surprisingly, even slightly better. This may be due to the fact that the EM algorithm estimates the component parameters accurately and also adapts to the data set. The three soft assignment methods perform similarly.

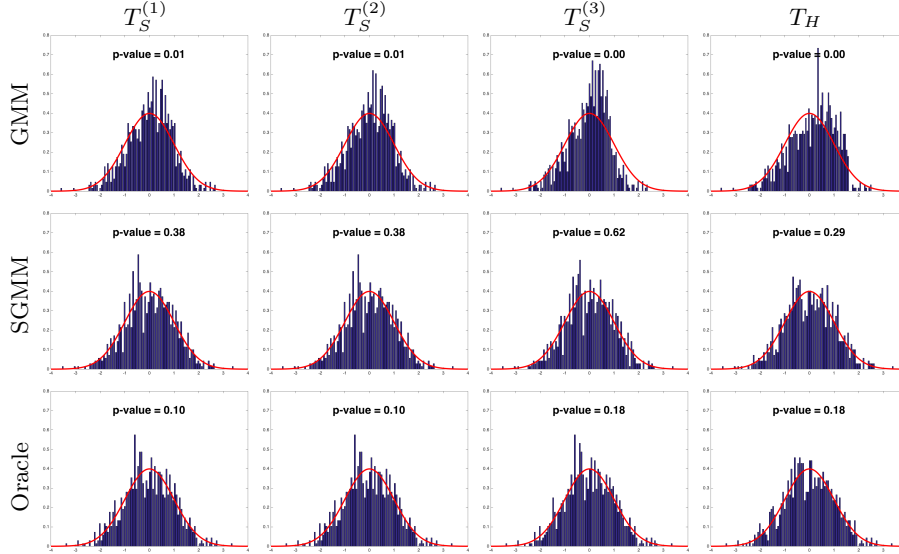
Fig 7: Simulated relative size $R(0.01)$ at the right tail for the univariate case. Each column corresponds to a different standardization method (three soft assignments and one hard assignment), while the three rows correspond to three parameter estimation methods (GMM, SGMM and oracle). The x -axis in each plot is the location t .



To further emphasize the distinction between the distribution of the standardized scores at *each* location presented above from that *across* locations, Figure 8 shows histograms of the latter for a single simulated realization. Except for the standard GMM method, most histograms match the standard normal distribution closely and are indistinguishable from it according to the Kolmogorov-Smirnov normality test.

4.2. Bivariate Data. In this section, we conduct simulations for bivariate data ($p = 2$), where the two scans correspond to the baseline (BL) and week-1 (W1) scans. We generate data from model (2.1) and (3.2) with $K = 3$, where the three classes correspond to GM, WM and CSF respectively. We use the probability maps provided by the software SPM as the population membership probability templates, allowing us to generate PET-like images. The template weights are given as $\gamma = (0.94, 0.01, 0.05)$ and the parameters

Fig 8: Histograms of standardized scores across locations from a single simulated realization. Each column corresponds to a different standardization method (three soft assignments and one hard assignment), while the three rows correspond to three parameter estimation methods (GMM, SGMM and oracle). The p-value in each plot is computed using a Kolmogorov-Smirnov normality test.

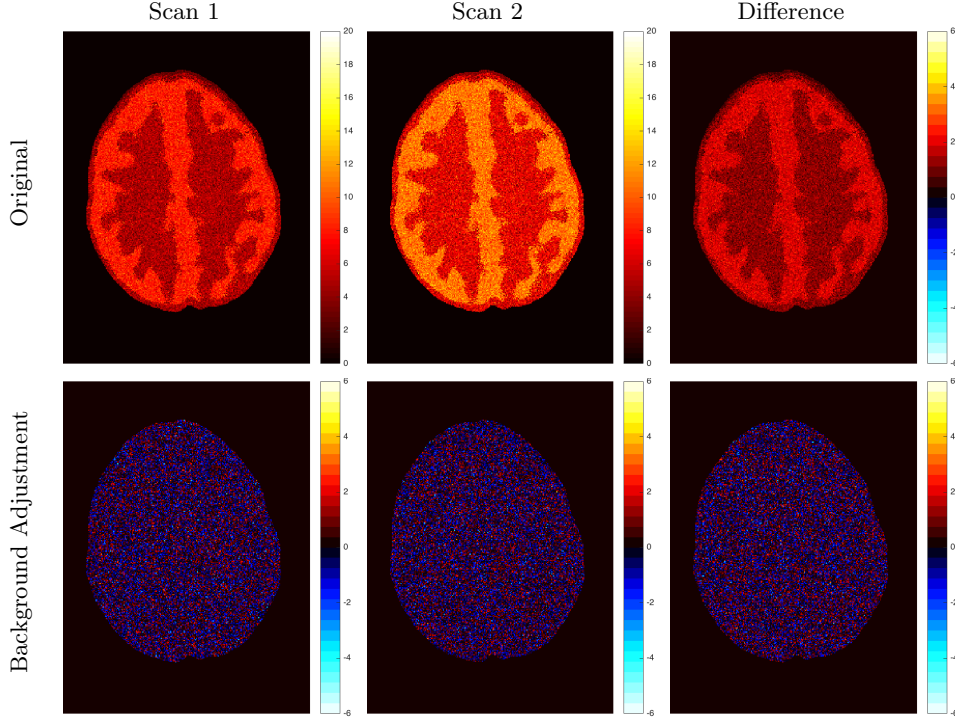


for each class are specified as

$$\begin{aligned}
 \mu_1 &= (4.91, 6.68)^T, & \mu_2 &= (8.04, 10.77)^T, & \mu_3 &= (2.76, 3.71)^T; \\
 \Sigma_1 &= \begin{pmatrix} 1.23 & 1.63 \\ 1.63 & 2.21 \end{pmatrix}, & \Sigma_2 &= \begin{pmatrix} 1.28 & 1.34 \\ 1.34 & 1.61 \end{pmatrix}, & \Sigma_3 &= \begin{pmatrix} 0.24 & 0.31 \\ 0.31 & 0.44 \end{pmatrix}.
 \end{aligned}$$

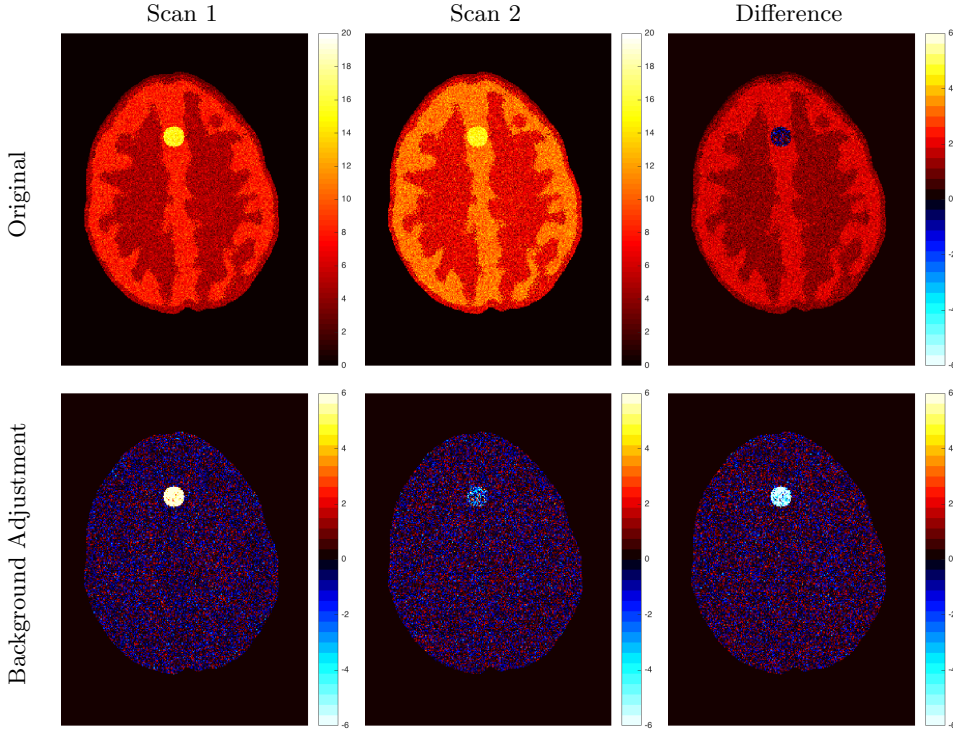
These parameters are close to the values that are obtained by applying the proposed robust EM algorithm to the real data (see Section 5 below). Focusing on a single slice for simplicity, each simulated PET scan is a 320 by 256 matrix where each pixel is a unit square. We consider two scenarios: (A) a PET image without lesions and (B) a PET image with a lesion. For Scenario B, a lesion in the shape of a circle with radius equal to 10 pixels is added, where the intensity at each pixel follows a $N(15, 1^2)$ distribution independently. Figures 9 and 10 plot an example for each scenario. Background adjustment is performed using soft assignment with the transformation $T_S^{(1)}$. (Additional simulations considering other lesion sizes and shapes are included in the Supplementary Materials.)

Fig 9: Simulated observations and background adjustment effects for Scenario A (no lesion). The 1st row shows the simulated original scans and the corresponding contrast, showing a global non-homogeneous background change. The 2nd row shows the respective standardized images via background adjustment and their difference. The adjusted observations and background difference are now randomly distributed around zero.



We first investigate the performance of all the three methods (i.e., traditional GMM, SGMM and RB-SGMM) in terms of parameter estimation for both scenarios. We use the following metrics to evaluate the differences between the estimated parameters and the true parameters: the Euclidean norm is used for the means and the 2-norm (i.e. maximum singular value of the difference between two matrices) is used for the covariance matrices and probability template map matrices $\pi = \{\pi_{ik}\}$. The results aggregating 1000 simulated instances are reported in Tables 1. The proposed SGMM and RB-SGMM are almost uniformly better than the traditional GMM for all parameters (except for Σ_2 in Scenario B where SGMM is slightly worse than GMM). This is expected since SGMM and RB-SGMM use the spatial

Fig 10: Simulated observations and background adjustment effects for Scenario B (lesion). The 1st row shows the simulated original scans and the corresponding contrast, showing a global non-homogeneous background change and little change in the lesion. The 2nd row shows the respective standardized images via background adjustment and their difference. The adjusted observations and background difference are now randomly distributed around zero and the lesion change is clearly visible.



population probability maps as priors while GMM uses constant probability maps. We also observe that RB-SGMM leads to similar accuracy compared to SGMM when there are no lesions in the observation (Scenario A in Table 1) and is much better than SGMM when there are lesions, i.e., outliers (Scenario B in Table 1). This indicates that the proposed RB-SGMM is preferred in applications since it is accurate without outliers but robust when outliers are present.

To better appreciate the distribution of the standardized scores, Figure 11 plots the density contour plots of the two scans from a single simulation. While the standardized scores $T_S^{(1)}$ are obtained using soft assignment, the

TABLE 1

Performance of the three methods GMM (Gaussian Mixture Models), SGMM (Spatial GMM) and RB-SGMM (robust SGMM) in terms of parameter estimation in Scenarios A and B. The norms of the differences between the estimated parameters and the true parameters are reported, below which is the standard error multiplied by 100 (in parenthesis).

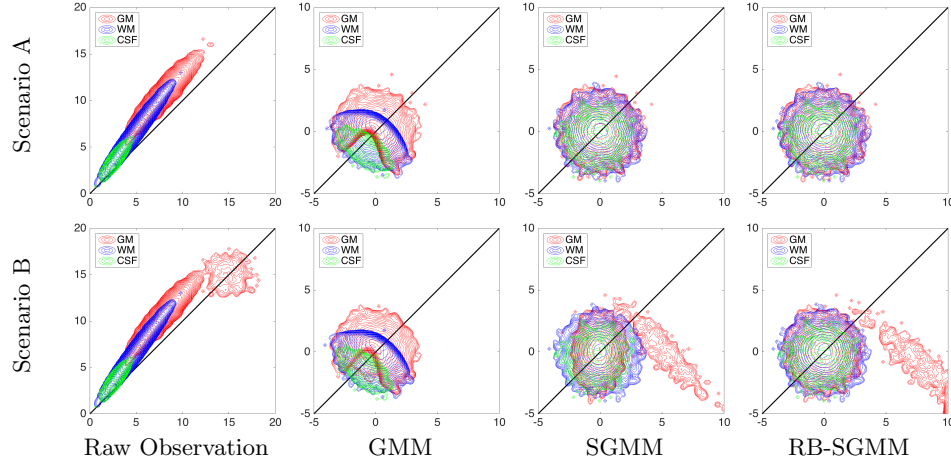
Method	Scenario A							Scenario B						
	μ_1	μ_2	μ_3	Σ_1	Σ_2	Σ_3	π	μ_1	μ_2	μ_3	Σ_1	Σ_2	Σ_3	π
GMM	2.42	3.39	5.46	0.80	0.54	2.23	122.56	6.26	4.57	9.63	1.29	1.13	2.24	139.44
SE ($\times 10^{-2}$)	(6.53)	(8.58)	(8.80)	(1.37)	(1.48)	(2.21)	(22.81)	(16.32)	(10.48)	(17.40)	(2.51)	(2.39)	(3.36)	(49.69)
SGMM	0.01	0.01	0.03	0.04	0.03	0.03	1.58	0.03	0.19	0.03	0.08	1.39	0.03	1.44
SE ($\times 10^{-2}$)	(0.03)	(0.03)	(0.06)	(0.08)	(0.06)	(0.07)	(2.01)	(0.05)	(0.04)	(0.06)	(0.12)	(0.11)	(0.07)	(1.88)
RB-SGMM	0.01	0.01	0.02	0.06	0.03	0.03	1.63	0.01	0.07	0.02	0.04	0.21	0.03	0.83
SE ($\times 10^{-2}$)	(0.03)	(0.03)	(0.06)	(0.11)	(0.07)	(0.07)	(2.01)	(0.03)	(0.04)	(0.05)	(0.09)	(0.10)	(0.07)	(1.38)

three classes are separated in the plots by hard assignment to ease visualization. In Scenario A, we can see that the original simulated observation has a mixture structure with correlation, while the standardized scores are given a distribution close to bivariate standard normal by the SGMM and RB-SGMM methods (first row, last two columns). The GMM method fails to do so because of the lack of use of spatial information and the inaccurate parameter estimates in Table 1. The RB-SGMM method shows its advantage over the SGMM method in Scenario B, offering better standardization (particularly in the grey matter) and better separation of the tumor pixels (second row, last two columns).

While Figure 11 describes the distribution of the standardized scores across voxels, it is important to make sure that the tail probabilities dictated by the standard normal distribution is also valid at each voxel. To show this, we study the tail probabilities of $a^T T_S^{(1)}$ in Scenario A using the contrast $a = (-1, 1)^T / \sqrt{2}$, which is the one of interest in the data analysis. Similar to Section 2.5, we evaluate the tail probabilities numerically using Monte Carlo simulation with 10^5 replications at level $\alpha = 0.01$.

Figure 12 plots the size ratio $R(0.01)$ at the left tail of the distribution of $a^T T_S^{(1)}$ using the true parameters (oracle) and the estimated parameters via GMM and SGMM. Panel (a) shows that the size ratio is very close to or smaller than 1 for almost all combinations of (π_1, π_2) (note that $\pi_1 + \pi_2 = 1 - \pi_3 \leq 1$). As expected from the univariate simulation results in Figure 7, the GMM method (panel (b)) gives very conservative size ratios whose location depend highly on the anatomical region (in this case the white matter). In contrast, given the estimation accuracy of the SGMM method shown in Table 1, it is not surprising that the voxelwise size ratios using SGMM (panel (c)) are very close to 1 for almost all voxels, being slightly conservative mainly in the thin transition region between the gray and white

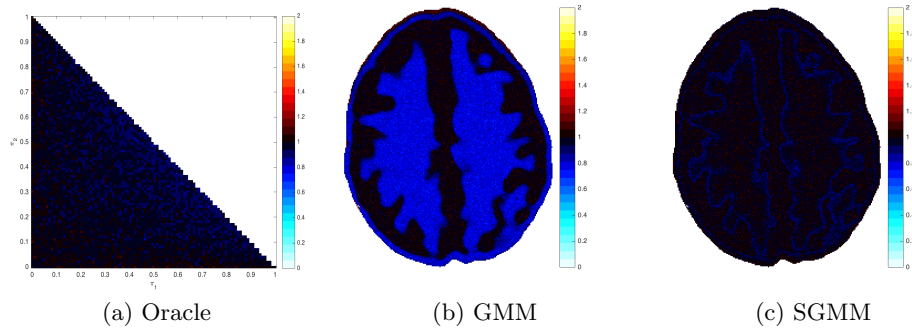
Fig 11: Bivariate density contour plots of the observations with and without soft background adjustment within each class. The first column is for the original simulated observations, while the last three columns are the scores after background adjustment using the methods GMM, SGMM and RB-SGMM respectively. The two rows correspond to Scenarios A and B.



matter. This suggests that the standardized scores obtained via SGMM and soft assignment are valid for statistical inference according to the standard normal at each voxel, as desired. The results for hard assignment are very similar (not shown).

5. PET data application. In this section, we provide more details about the PET data application discussed in the Introduction (Figure 1). We use the data produced by the lesion change detection study in (Qin et al., 2017) using the Hoffman 3-D brain phantom (Hoffman et al., 1991), which simulates pre- and post-treatment scans with a tumor lesion. As described there, the brain phantom was filled with FDG radioactive fluid and PET scans were acquired on a GE Discovery ST PET-CT scanner. A malignant lesion was simulated within the central gray matter at a location superior and anterior within the brain, by placing a 1.5 cm diameter sphere of FDG. The tumor-to-background-ratio (TBR) for Scan 1 was 2:1, which was changed to 1.5:1 for Scan 2. Due to the physical construction of the phantom, these two TBR levels were achieved by increasing the activity in the phantom background rather than changing the activity in the lesion (injecting more radio-tracer to the background, while keeping the activity concentration in the lesion constant), effectively producing a reduction in

Fig 12: Heatmaps of the size ratio $R(0.01)$ (left-side tail) for the bivariate simulations in Section 4.2 with soft assignment: using the true parameters under various combinations of (π_1, π_2) (a); using the estimated parameters by GMM (b) and SGMM (c).

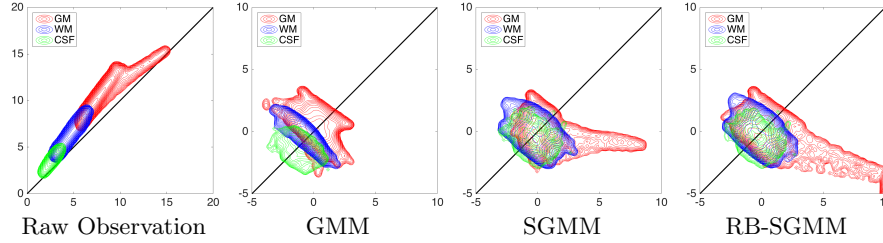


the lesion activity with respect to the background. Image registration was performed between the two scans. The first row of Figure 1 shows one slice of the two scans and their difference (same slice as in Qin et al. (2017)).

By design, there is a large background change but no change in the lesion. A direct difference between the two scans shows a global non-homogeneous background change while failing to detect changes in the lesion (Figure 1, Row 1 and Column 3). In contrast, the analysis based on the model-based standardized differences proposed in this paper is successful (Figure 1, Row 2 and Column 3). Specifically, the second row shows the standardized scores using the proposed robust EM algorithm RB-SGMM and background adjustment via the soft-assignment transformation $T_S^{(1)}$. The estimated background parameters are those given in (4.1). The standardized scores show a distribution close to standard normal with little anatomical structure except for the lesion. The standardized difference in the third column again has a distribution close to standard normal and exhibits the lesion change clearly at -6 standard deviations away from 0.

To better appreciate the distributions, Figure 13 plots the density contours of the original observations and standardized scores for the three estimation methods considered in this paper. As in Figure 11, while the standardized scores $T_S^{(1)}$ are obtained using soft assignment, the three classes are separated in the plots by hard assignment to ease visualization. Compared to GMM and SGMM, the robust RB-SGMM method offers the best standardization and separation of the pixels corresponding to the lesion.

Fig 13: Bivariate density contour plots of the phantom data with and without soft background adjustment within each class. The first column is for the original observation, while the last three columns are the scores after background adjustment using the methods of GMM, SGMM and RB-SGMM respectively.



6. Discussion. In this paper, we addressed the background adjustment problem in brain image analysis where there is interest in detecting outliers (i.e., tumor lesions) against the mixture model background. This problem motivated a robust EM algorithm to estimate the model parameters in a spatial Gaussian mixture model and standardization methods for background adjustment using both soft and hard assignment. We found that the proposed RB-SGMM method using soft assignment is justified for the purpose of hypothesis testing in the sense that tail probabilities at each voxel tend to be equal or smaller than those of the standard normal, thereby making testing accurate or conservative in a variety of scenarios.

In terms of standardization, we found that the differences in performance between $T_S^{(1)}$, $T_S^{(2)}$ and $T_S^{(3)}$ are small, as long as soft assignment is used. We generally prefer $T_S^{(1)}$ because of its ease of analysis (it depends on a lower dimensional parameter space) and slightly better performance, and is the default method in the software package **RB-SGMM-BA**. Hard assignment is less reliable, performing worse than soft assignment for some mixture parameter combinations. For univariate data, there exists the possibility of applying a quantile transformation as a way of transforming the observed mixture variables to standard normal. We did not consider the quantile transformation here because it does not have an obvious extension to bivariate or multivariate data, which has been the focus of this paper. Other simulations, not presented here, indicate that the quantile transformation for univariate data may be very sensitive to the estimates of the class-belonging probabilities π_{ik} and yield undesired anti-conservative tail probabilities.

Including a robust step in the SGMM algorithm to create RB-SGMM

has been found to be critical. To create RB-SGMM, we modified the EM algorithm of [Ashburner and Friston \(2005\)](#) in such a way that we kept the number of classes in the mixture to represent the major tissue types, but made the M step robust to outliers. The proposed robust method replaces that of [Qin et al. \(2017\)](#), which iteratively re-estimated the mixture parameters from observations whose standardized scores, after applying the contrast of interest, were in absolute value less than a constant c (they used $c = 2$). While also iterative, our proposed robust estimation is based on the theory of M-estimation and the EM algorithm, yielding accurate results. The use of a continuous weight function $\min(s, k_1(p))/s$ in the M-estimators is preferable to the discontinuous weight function that would correspond to the method of [Qin et al. \(2017\)](#) and is less sensitive to the tuning parameter $k_1(p)$ than to the constant c . A more sophisticated model could allow the tissue-belonging probabilities π_{ik} to be modified not only according to regular anatomical variation via the γ_k coefficients in (3.2) but also due to the anatomical deformations produced by the lesions themselves. A possible combination of SGMM and GMM including a non-spatial component for lesions may be an idea to consider in future work.

Although tailored to brain image analysis, we emphasize that the developed standardization of GMM with robust estimation may be applicable to other settings (e.g., genomics), where there is interest in detecting signal against a mixture background.

SUPPLEMENTARY MATERIAL

Supplement: Additional material

(doi: [ATTACHED TO THIS FILE](#); .pdf). Supplementary materials contain: (A) proofs of all theorems and lemmas in the main paper; (B) a simulation study to compare the proposed robust EM with the multivariate t mixtures method ([Peel and McLachlan, 2000](#)) in a non-spatial setting; (C) additional simulation studies of the proposed RB-SGMM approach when lesions have smaller sizes and are non-circular.

References.

- Ashburner, J. (2012). SPM: A history. *NeuroImage*, 62(2):791–800.
- Ashburner, J. and Friston, K. J. (2005). Unified segmentation. *Neuroimage*, 26(3):839–851.
- Bai, B., Bading, J., and Conti, P. S. (2013). Tumor quantification in clinical positron emission tomography. *Theranostics*, 3(10):787–801.
- Besag, J. (1986). On the statistical analysis of dirty pictures. *Journal of the Royal Statistical Society. Series B (Statistical Methodology)*, 48(3):259–302.
- Borghammer, P., Aanerud, J., and Gjedde, A. (2009). Data-driven intensity normalization of PET group comparison studies is superior to global mean normalization. *Neuroimage*, 46(4):981–988.

- Campbell, N. A. (1984). Mixture models and atypical values. *Mathematical Geology*, 16:465–477.
- Chen, J. L., Gunn, S. R., Nixon, M. S., and Gunn, R. N. (2001). Markov random field models for segmentation of PET images. In *Biennial International Conference on Information Processing in Medical Imaging*, pages 468–474. Springer.
- Dasgupta, A., Hopcroft, J., Kleinberg, J., and Sandler, M. (2005). On learning mixtures of heavy-tailed distributions. In *46th Annual IEEE Symposium on Foundations of Computer Science (FOCS'05)*, pages 491–500. IEEE.
- Dempster, A. P., Laird, N. M., and Rubin, D. B. (1977). Maximum likelihood from incomplete data via the EM algorithm. *Journal of the Royal Statistical Society. Series B (Statistical Methodology)*, 39(1):1–38.
- Devlin, S. J., Gnanadesikan, R., and Kettenring, J. R. (1981). Robust estimation of dispersion matrices and principal components. *Journal of the American Statistical Association*, 76(374):354–362.
- Figueiredo, M. A. T. and Jain, A. K. (2002). Unsupervised learning of finite mixture models. *IEEE Transactions on Pattern Analysis and Machine Intelligence*, 24(3):381–396.
- Guo, M., Yap, J. T., den Abbeele, A. D., Lin, N. U., and Schwartzman, A. (2014). Voxel-wise single-subject analysis of imaging metabolic response to therapy in neuro-oncology. *Stat*, 3(1):172–186.
- Gupta, M. R. and Chen, Y. (2011). *Theory and use of the EM algorithm*. Now Publishers Inc.
- Hanson, T. E. (2006). Inference for mixtures of finite Polya tree models. *Journal of the American Statistical Association*, 101(476):1548–1565.
- Hoffman, E. J., Cutler, P. D., Guerrero, T. M., Digby, W. M., and Mazziotta, J. C. (1991). Assessment of accuracy of PET utilizing a 3-D phantom to simulate the activity distribution of [18F] fluorodeoxyglucose uptake in the human brain. *Journal of Cerebral Blood Flow & Metabolism*, 11:A17—A25.
- Huber, P. J. (1964). Robust Estimation of a Location Parameter. *Annals of Mathematical Statistics*, 35(1):73–101.
- Leahy, R. M. and Qi, J. (2000). Statistical approaches in quantitative positron emission tomography. *Statistics and Computing*, 10(2):147–165.
- Lee, Y.-Y., Choi, C. H., Kim, C. J., Kang, H., Kim, T.-J., Lee, J.-W., Lee, J.-H., Bae, D.-S., and Kim, B.-G. (2009). The prognostic significance of the SUVmax (maximum standardized uptake value for F-18 fluorodeoxyglucose) of the cervical tumor in PET imaging for early cervical cancer: preliminary results. *Gynecologic oncology*, 115(1):65–68.
- Lin, T. I., Lee, J. C., and Yen, S. Y. (2007). Finite mixture modelling using the skew normal distribution. *Statistica Sinica*, 17(3):909–927.
- Lo, Y., Mendell, N. R., and Rubin, D. B. (2001). Testing the number of components in a normal mixture. *Biometrika*, 88(3):767–778.
- Maronna, R. A. (1976). Robust M-Estimators of Multivariate Location and Scatter. *The Annals of Statistics*, 4(1):51–67.
- Maronna, R. A., Martin, R. D., and Yohai, V. J. (2006). *Robust Statistics*. Wiley Series in Probability and Statistics. John Wiley & Sons, Ltd, Chichester, UK.
- McLachlan, G. and Peel, D. (2000). *Finite Mixture Models*. Wiley Series in Probability and Statistics. Wiley-Interscience, New York.
- McLachlan, G. J. and Basford, K. E. (1988). *Mixture models: Inference and applications to clustering*. Marcel Dekker, New York.
- McLachlan, G. J. and Krishnan, T. (2008). *The EM Algorithm and Extensions*. Wiley

- Series in Probability and Statistics. John Wiley & Sons, Inc., Hoboken, NJ, USA, second edition.
- O’Sullivan, F., Muzi, M., Mankoff, D. A., Eary, J. F., Spence, A. M., and Krohn, K. A. (2014). Voxel-level mapping of tracer kinetics in PET studies: A statistical approach emphasizing tissue life tables. *The Annals of Applied Statistics*, 8(2):1065–1094.
- Peel, D. and McLachlan, G. J. (2000). Robust mixture modelling using the t distribution. *Statistics and Computing*, 10(4):339–348.
- Qin, L., Schwartzman, A., McCall, K., Kachouie, N. N., and Yap, J. T. (2017). Method for detecting voxelwise changes in fluorodeoxyglucose-positron emission tomography brain images via background adjustment in cancer clinical trials. *Journal of Medical Imaging*, 4(2):024006.
- Qin, Y. and Priebe, C. E. (2013). Maximum L_q-Likelihood Estimation via the Expectation-Maximization Algorithm: A Robust Estimation of Mixture Models. *Journal of the American Statistical Association*, 108(503):914–928.
- Redner, R. A. and Walker, H. F. (1984). Mixture densities, maximum likelihood and the EM algorithm. *SIAM review*, 26(2):195–239.
- Richardson, S. and Green, P. J. (1997). On Bayesian analysis of mixtures with an unknown number of components (with discussion). *Journal of the Royal Statistical Society: Series B (Statistical Methodology)*, 59(4):731–792.
- Sanjay-Gopal, S. and Hebert, T. (1998a). Bayesian pixel classification using spatially variant finite mixtures and the generalized EM algorithm. *IEEE Transactions on Image Processing*, 7(7):1014–1028.
- Sanjay-Gopal, S. and Hebert, T. J. (1998b). Bayesian pixel classification using spatially variant finite mixtures and the generalized EM algorithm. *IEEE Transactions on Image Processing*, 7(7):1014–1028.
- Soffientini, C. D., De Bernardi, E., Zito, F., Castellani, M., and Baselli, G. (2016). Background based Gaussian mixture model lesion segmentation in PET. *Medical Physics*, 43(5):2662–2675.
- Soret, M., Bacharach, S. L., and Buvat, I. (2007). Partial-volume effect in PET tumor imaging. *Journal of Nuclear Medicine*, 48(6):932–945.
- Stephens, M. (2000). Bayesian analysis of mixture models with an unknown number of components: an alternative to reversible jump methods. *The Annals of Statistics*, 28(1):40–74.
- Takeda, A., Yokosuka, N., Ohashi, T., Kunieda, E., Fujii, H., Aoki, Y., Sanuki, N., Koike, N., and Ozawa, Y. (2011). The maximum standardized uptake value (SUV_{max}) on FDG-PET is a strong predictor of local recurrence for localized non-small-cell lung cancer after stereotactic body radiotherapy (SBRT). *Radiotherapy and Oncology*, 101(2):291–297.
- Thanh Minh Nguyen and Wu, Q. M. J. (2012). Gaussian-Mixture-Model-Based Spatial Neighborhood Relationships for Pixel Labeling Problem. *IEEE Transactions on Systems, Man, and Cybernetics, Part B (Cybernetics)*, 42(1):193–202.
- Valk, P. E., Bailey, D. L., Townsend, D. W., and Maisey, M. N. (2003). *Positron emission tomography: basic science and clinical practice*. Springer London.
- Vehtari, A. and Ojanen, J. (2012). A survey of Bayesian predictive methods for model assessment, selection and comparison. *Statistics Surveys*, 6(August):142–228.
- Venturini, S., Dominici, F., and Parmigiani, G. (2008). Gamma shape mixtures for heavy-tailed distributions. *The Annals of Applied Statistics*, 2(2):756–776.
- Vlassis, N. and Likas, A. (1999). A kurtosis-based dynamic approach to Gaussian mixture modeling. *IEEE Transactions on Systems, Man, and Cybernetics-Part A: Systems and Humans*, 29(4):393–399.

- Wahl, R. L., Jacene, H., Kasamon, Y., and Lodge, M. A. (2009). From RECIST to PERCIST: evolving considerations for PET response criteria in solid tumors. *Journal of Nuclear Medicine*, 50(Suppl 1):122S–150S.
- Young, H., Baum, R., Cremerius, U., Herholz, K., Hoekstra, O., Lammertsma, A. A., Pruim, J., Price, P., and Others (1999). Measurement of clinical and subclinical tumour response using [18 F]-fluorodeoxyglucose and positron emission tomography: review and 1999 EORTC recommendations. *European Journal of Cancer*, 35(13):1773–1782.
- Zasadny, K. R. and Wahl, R. L. (1993). Standardized uptake values of normal tissues at PET with 2-[fluorine-18]-fluoro-2-deoxy-D-glucose: variations with body weight and a method for correction. *Radiology*, 189(3):847–850.
- Zhang, J., Modestino, J. W., and Langan, D. A. (1994). Maximum-likelihood parameter estimation for unsupervised stochastic model-based image segmentation. *IEEE Transactions on Image Processing*, 3(4):404–420.

Supplementary Materials to “Standardization of multivariate Gaussian mixture models and background adjustment of PET images in brain oncology”

A Proofs

Proof of Theorem 2.1. We first consider the transformation with the hard assignment T_H .

Part 1). If $\pi_1 \rightarrow 1$, then it follows that $s_1 \xrightarrow{p} 1$, $r(Y) = O_p(1)$ and $\pi_0 \rightarrow -\infty$. Therefore, we have $\tilde{s}_1 = \mathbb{1}(r(Y) > \pi_0) \xrightarrow{p} 1$, and thus $\mathbb{1}(\tilde{s}_1 = s_1) \xrightarrow{p} 1$. By applying (11), we obtain that $T_H - Z = O_p(1) \cdot \mathbb{1}(\tilde{s}_1 \neq s_1) = o_p(1)$, which concludes the proof. Similar argument follows when $\pi_2 \rightarrow 1$.

Part 2). According to the result in (10), it is easy to obtain that when $s_1 = 1$, $r(Y) \rightarrow +\infty$ with probability 1 and when $s_2 = 1$, $r(Y) \rightarrow -\infty$ with probability 1. Therefore, when $s_1 = 1$, we have $\tilde{s}_1 = 1$ with probability 1; when $s_2 = 1$, we have $\tilde{s}_2 = 1$ with probability 1. Consequently, it follows that $\tilde{s}_1 - s_1 \xrightarrow{a.s.} 0$ and thus $T_H \xrightarrow{a.s.} Z$ by applying the result in (11).

Part 3) and 4), we obtain that $T_H \xrightarrow{a.s.} Z$ by applying the result in (11) directly.

Then we consider the case when the soft assignment is used, i.e., the transformation $T_S^{(1)}$. Under conditions in part 1) and 2), we note that $w_1(1-w_1) \xrightarrow{a.s.} 0$. This implies the asymptotic equivalence between the soft and hard assignment and thus the conclusions established for T_H hold for $T_S^{(1)}$. For part 3) and 4), we have $T_S^{(1)} \xrightarrow{a.s.} Z$ by applying (8) directly. \square

Proof of Theorem 2.5. Note that the map g is a bijection and the corresponding inverse map is $g^{-1} : \mathbb{R}^p \rightarrow \mathbb{R}^p$, $g^{-1}(x) = \tau^{-1}x - \Delta_1$. According to the definitions of g and h , we can represent $r(Y)$ in (10) as $r(Y) = h(Z) \cdot \mathbb{1}(s_1 = 1) + h(g^{-1}(Z)) \cdot \mathbb{1}(s_2 = 1)$. Furthermore, the result in (11) gives that $T_H = Z \cdot \mathbb{1}(\tilde{s}_1 = s_1) + g^{-1}(Z) \cdot \mathbb{1}(\tilde{s}_1 > s_1) + g(Z) \cdot \mathbb{1}(\tilde{s}_1 < s_1)$.

If $s_1 = 1$, the event $\{\tilde{s}_1 = 1\} = \{r(Y) > \pi_0\} = \{h(Z) > \pi_0\} = \{Z : Z \in R_3^c\}$ with probability 1. Consequently, we have

$$\begin{aligned} P(a^T T_H \leq t | s_1 = 1) &= P(a^T T_H \leq t, \tilde{s}_1 = 1 | s_1 = 1) + P(a^T T_H \leq t, \tilde{s}_2 = 1 | s_1 = 1) \\ &= P(a^T Z \leq t, \tilde{s}_1 = 1 | s_1 = 1) + P(a^T g(Z) \leq t, \tilde{s}_2 = 1 | s_1 = 1) \\ &= P(a^T Z \leq t, Z \in R_3^c | s_1 = 1) + P(a^T g(Z) \leq t, Z \in R_3 | s_1 = 1). \end{aligned}$$

Since Z and s_1 are independent, it follows that

$$P(a^T T_H \leq t | s_1 = 1) = P(a^T Z \leq t, Z \in R_3^c) + P(a^T g(Z) \leq t, Z \in R_3),$$

which is $\Phi_p(R_2 \cap R_3^c) + \Phi_p(g^{-1}(R_2) \cap R_3)$. Because Z is multivariate standard normal and a has unit Euclidean norm, the random variable $a^T Z$ is thus standard normal. Therefore, we have $\Phi(t) = P(a^T Z < t) = \Phi_p(R_2)$, yielding that

$$P(a^T T_H \leq t | s_1 = 1) - \Phi(t) = \Phi_p(g^{-1}(R_2) \cap R_3) - \Phi_p(R_2 \cap R_3).$$

Following the same argument, if $s_2 = 1$, the event $\{\tilde{s}_1 = 1\} = \{Z : h(g^{-1}(Z)) > \pi_0\} = \{Z : Z \in g(R_3^c)\}$ with probability 1, and thus we have

$$\begin{aligned} P(a^T T_H \leq t | s_2 = 1) &= P(a^T T_H \leq t, \tilde{s}_1 = 1 | s_2 = 1) + P(a^T T_H \leq t, \tilde{s}_2 = 1 | s_2 = 1) \\ &= P(a^T g^{-1}(Z) \leq t, Z \in g(R_3^c)) + P(a^T Z \leq t, Z \in g(R_3)) \\ &= \Phi_p(g(R_2) \cap g(R_3^c)) + \Phi_p(R_2 \cap g(R_3)), \end{aligned}$$

where the property of $g(R_3^c) = g(R_3)^c$ is used. We thus have $P(a^T T_H \leq t | s_2 = 1) - \Phi(t) = \Phi_p(g(R_2) \cap g(R_3^c)) - \Phi_p(R_2 \cap g(R_3^c))$. Consequently, $P(a^T T_H \leq t) - \Phi(t)$ is equal to

$$\begin{aligned} &[P(a^T T_H \leq t | s_1 = 1) - \Phi(t)]P(s_1 = 1) + [P(a^T T_H \leq t | s_2 = 1) - \Phi(t)]P(s_2 = 1) \\ &= \pi_1[\Phi_p(g^{-1}(R_2) \cap R_3) - \Phi_p(R_2 \cap R_3)] + \pi_2[\Phi_p(g(R_2) \cap g(R_3^c)) - \Phi_p(R_2 \cap g(R_3^c))], \end{aligned}$$

which concludes the proof. \square

Proof of Lemma 2.6. When $\tau > 1$, we have $h(x) - \pi_0 = (\tau^2 - 1) \left(x + \frac{\tau \Delta_2}{\tau^2 - 1}\right)^2 - \frac{c_0}{\tau^2 - 1}$, according to the definition of h and c_0 .

If $c_0 > 0$, it is easy to check that $(a_{\pm}(\theta))$ in (12a) are the two roots of the equation $h(x) = \pi_0$. Therefore, the set $R_3 = \{h(x) < \pi_0\} = (a_-(\theta), a_+(\theta))$. If $c_0 \leq 0$, we have $\tau > 1$ because otherwise $\tau = 1$ and $\Delta_2 = 0$, which leads to $\theta \in \Theta_0$. In this case, the set $R_3 = \emptyset$, which is $(a_-(\theta), a_+(\theta))$ since $a_-(\theta)$ is equal to $a_+(\theta)$.

If $c_0 > 0$ and $\tau = 1$, the quadratic equation $h(x) - \pi_0 = 0$ degenerates to a linear equation. Specifically, we have $h(x) - \pi_0 = 2\Delta_2 x + \Delta_2^2 - \pi_0$. Therefore, we have $R_3 = (\pi_0/(2\Delta_2) - \Delta_2/2, +\infty)$ if $\Delta_2 > 0$, and $R_3 = (-\infty, \pi_0/(2\Delta_2) - \Delta_2/2)$ if $\Delta_2 < 0$. \square

Proof of Theorem 2.8. For the univariate case when $p = 1$, the set R_2 in Theorem 2.5 is $(-\infty, t)$ since the contrast coefficient a is 1. For any $a \leq b \in \mathbb{R}$, we define

$$\begin{aligned} A(t, a, b) &= (-\infty, t) \cap ((-\infty, a) \cup (b, +\infty)) = (-\infty, t \wedge a) \cup (b, t \vee b) \\ B(t, a, b) &= (-\infty, t) \cap (a, b) = (a, a \vee (t \wedge b)), \end{aligned}$$

which leads to

$$\Phi(A(t, a, b)) = \Phi(t \wedge a) + \Phi(t \vee b) - \Phi(b); \quad \Phi(B(t, a, b)) = \Phi(a \vee (t \wedge b)) - \Phi(a).$$

According to Lemma 2.6, we have the set $R_3 = (a_-, a_+)$. It follows that $A(t, a_-, a_+) = R_2 \cap R_3^c$ and $B(t, a_-, a_+) = R_2 \cap R_3$. Let $b_- = g(a_-) = \tau a_- + \Delta_2$ and $b_+ = g(a_+) = \tau a_+ + \Delta_2$. By applying Theorem 2.5, we obtain that

$$\begin{aligned} P(T \leq t) - \Phi(t) &= \pi_1[\Phi(B(t/\tau - \Delta_1, a_-, a_+)) - \Phi(B(t, a_-, a_+))] \\ &\quad + \pi_2[\Phi(A(\tau t + \Delta_2, b_-, b_+)) - \Phi(A(t, b_-, b_+))] \\ &= \pi_1[\Phi((b_- \vee (t \wedge b_+))/\tau - \Delta_1) - \Phi(a_- \vee (t \wedge a_+))] \\ &\quad + \pi_2[\Phi(\tau(t \wedge a_-) + \Delta_2) + \Phi(\tau(t \vee a_+) + \Delta_2) - \Phi(t \wedge b_-) - \Phi(t \vee b_+)], \end{aligned}$$

which leads to the result in (13). \square

Proof of Lemma 2.9. We denote T in (8) as $T = g_1(Z, \Delta_1, \tau, \pi_0)s_1 + g_2(Z, \Delta_1, \tau, \pi_0)s_2$ to emphasize its dependency on $(Z, \Delta_1, \tau, \pi_0)$. Recall that Z is independent with (s_1, s_2) , therefore we have the conditional random variable $T|(s_1 = 1) = g_1(Z, \Delta_1, \tau, \pi_0)$. For both hard and soft assignments, \tilde{s}_1, \tilde{s}_2 is a function of $r(Y) - \pi_0$, and $r(Y)|(s_1 = 1) = (\tau Z + \tau \Delta_1)^T(\tau Z + \tau \Delta_1) - Z^T Z$. Therefore, it is easy to see that $g_1(Z, \Delta_1, \tau, \pi_0) = -g_1(-Z, -\Delta_1, \tau, \pi_0)$. Since Z and $-Z$ are identically distributed, we will have the same distribution for $|a^T T|(s_1 = 1)$ when we change Δ_1 to $|\Delta_1|$. Similarly, the distribution of $|a^T T|(s_2 = 1)$ depends on Δ_1 through the absolute values $|\Delta_1|$. Therefore, the distribution of $|T|$ depends on Δ_1 only through $|\Delta_1|$. This establishes the lemma. \square

B Comparison between RB-GMM and the multivariate t mixtures method

In this section, we compare the robust Gaussian mixture models via the M estimation in Section 3 with the multivariate t mixtures method (Peel and McLachlan, 2000). We do not consider the spatial structure and focus on comparing the performance of these two approaches in terms of robustness. We replace the M step in a traditional GMM by the robust M step detailed in Section 3, termed as RB-GMM. The multivariate t mixtures method is implemented in the R package **EMMIXuskew** (Lee and McLachlan, 2013), where the skewness parameters are set to be 0.

In the simulation, we simulate data using $K = 2$ clusters with the following parameter values

$$\mu_1 = \begin{pmatrix} 0 \\ 3 \end{pmatrix}, \quad \mu_2 = \begin{pmatrix} 3 \\ 0 \end{pmatrix}, \quad \Sigma_1 = \Sigma_2 = \begin{pmatrix} 1 & 0 \\ 0 & 1 \end{pmatrix}, \quad \pi_1 = 0.6, \quad \pi_2 = 0.4.$$

We generate $n = 100$ observations and 5% of them are outliers independently drawn from $N(15, 1)$. We implemented the Gaussian mixture model (GMM), the proposed robust GMM without spatial structures (RB-GMM), and the multivariate t mixtures method (MIX t). The table below reports the relative errors of each estimated parameter using the Euclidean norm for both the mean and π , and the 2-norm for the covariance matrices, averaged over 100 replications. The standard errors are reported in parenthesis.

Method	μ_1	μ_2	Σ_1	Σ_2	π
GMM	0.69 (0.11)	5.07 (0.24)	5.42 (1.31)	9.29 (1.62)	0.59 (0.03)
RB-GMM ($q = 70\%$)	0.07 (0.00)	0.12 (0.01)	0.45 (0.01)	0.68 (0.05)	0.11 (0.02)
RB-GMM ($q = 80\%$)	0.08 (0.00)	0.13 (0.01)	0.45 (0.02)	0.89 (0.06)	0.09 (0.01)
RB-GMM ($q = 90\%$)	0.11 (0.01)	0.60 (0.16)	0.73 (0.08)	1.87 (0.19)	0.13 (0.02)
MIX t	0.09 (0.01)	0.24 (0.09)	0.61 (0.08)	0.85 (0.15)	0.16 (0.02)

We can see that both RB-GMM and MIX t improve the estimation much compared to GMM. In addition, RB-GMM at $q = 70\%$ or 80% outperforms MIX t , but not so when $q = 90\%$. This suggests that if we tend to be conservative and use lower q (thus presume there are more outliers than needed), RB-GMM leads to much better estimation performance

at least under this simulation setting. Therefore, the approach of RB-GMM provides flexibility to incorporate prior knowledge about the proportion of outliers. In our brain imaging applications, the proportion of brain volume occupied by tumors is usually small (often less than 1%), thus we recommended to use $q = 99\%$ as the default threshold. The comparison between RB-GMM and *MIXt* is expected to depend on the settings, such as the deviation of the outliers from the two clusters. We observed that, compared to GMM and RB-GMM, the *MIXt* approach takes much longer to run, as the number of degrees of freedoms requires extra computation at each iteration of the EM algorithm. *MIXt* also seems more sensitive to the initial values of parameters. In fact, in this simulation we provided the true parameters as the initial values, mainly motivated by favoring *MIXt* and make it work, but benefiting all the three approaches in comparison.

One of the major contribution of this paper is to combine spatial structures of π with the robust EM procedure, which is tailored to the main application of biomedical imaging where template maps are indeed available and lesions often exist. We are not aware of whether the *MIXt* method has been generalized to this spatial setting. This may be viewed as a future research topic.

C Additional simulations comparing tumor size and shape

In this section, we conduct simulations following the settings in Section 4.2 but vary the tumor size and shape. We consider three additional scenarios and plot the background adjustment effects and bivariate density contours (similar to Figures 10 and 11): circular lesion with radius 6 in Figure 14, circular lesion with radius 3 in Figure 15, and a lesion formed as a union of two ellipses in Figure 16.

The performances of the proposed method are not affected by the lesion’s smaller size or different shape. In all three figures, the first row shows a global non-homogeneous background change and little change in the lesion, but the adjusted observations and background difference in the second row are randomly distributed around zero and the lesion change is clearly visible. The last row of contour plots shows that RB-SGMM offers a standardized score close to normal and isolates the lesion successfully. The observation that the proposed method is not sensitive to lesion size or shape is explained by the fact that the treatment of outliers follows a voxelwise approach, so the lesion size or shape have little effect if the background parameters are estimated robustly. While the estimation of the background depends on spatial templates, the treatment of outliers does not. This allows the use of valuable spatial information for the background and yet being very flexible regarding the unknown location, size or shape of the lesion.

Figure 14: Simulated observations and background adjustment effects for Scenario B when the radius of the lesion is 6. The 1st row shows the simulated original scans and the corresponding contrast. The 2nd row shows the respective standardized images via background adjustment and their difference. The last row shows bivariate density contour plots of the observations with and without soft background adjustment within each class. The first column is for the original simulated observations, while the last three columns are the scores after background adjustment using the methods GMM, SGMM and RB-SGMM respectively.

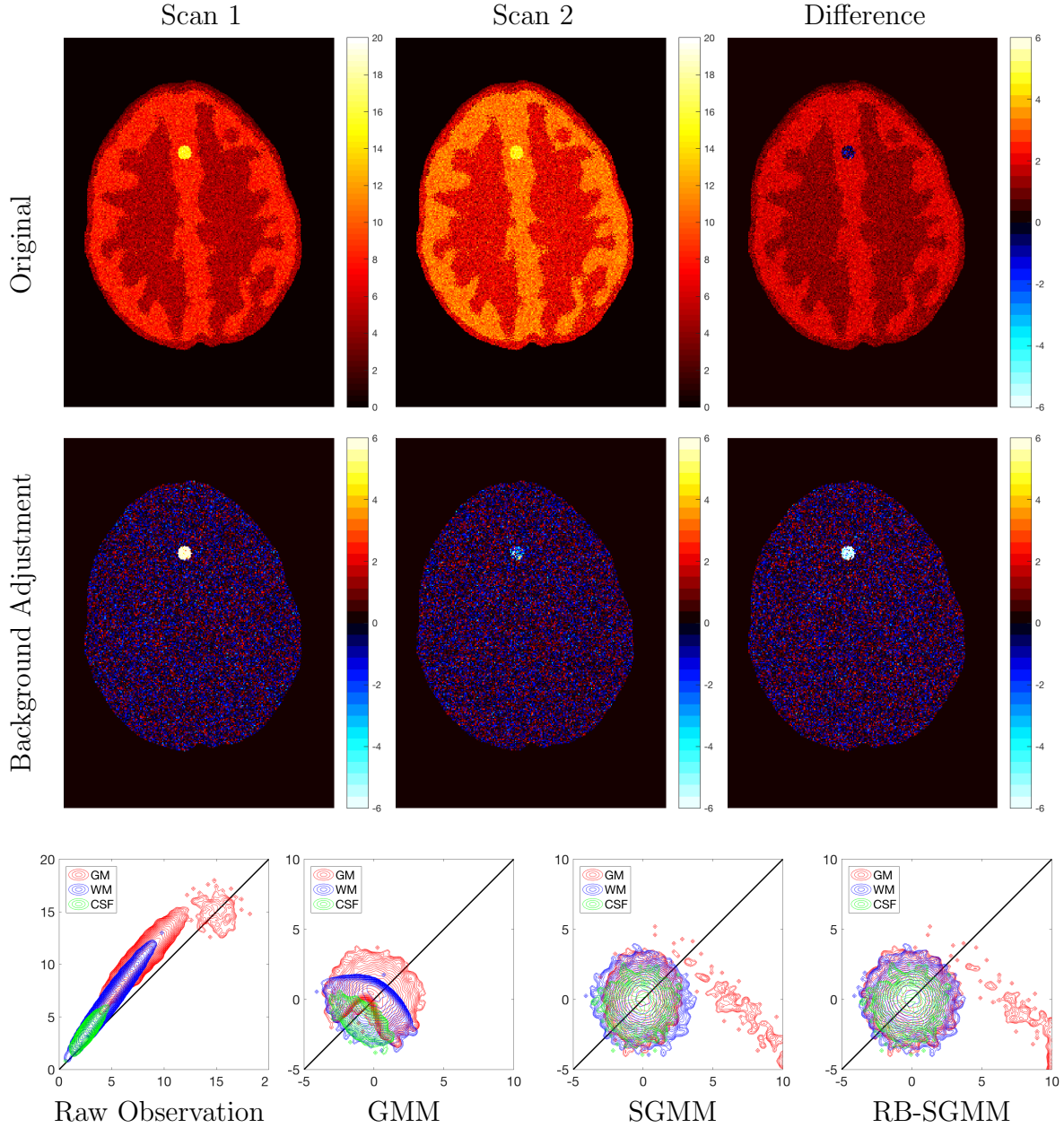


Figure 15: Simulated observations and background adjustment effects for Scenario B when the radius of the lesion is 3. The 1st row shows the simulated original scans and the corresponding contrast. The 2nd row shows the respective standardized images via background adjustment and their difference. The last row shows bivariate density contour plots of the observations with and without soft background adjustment within each class. The first column is for the original simulated observations, while the last three columns are the scores after background adjustment using the methods GMM, SGMM and RB-SGMM respectively.

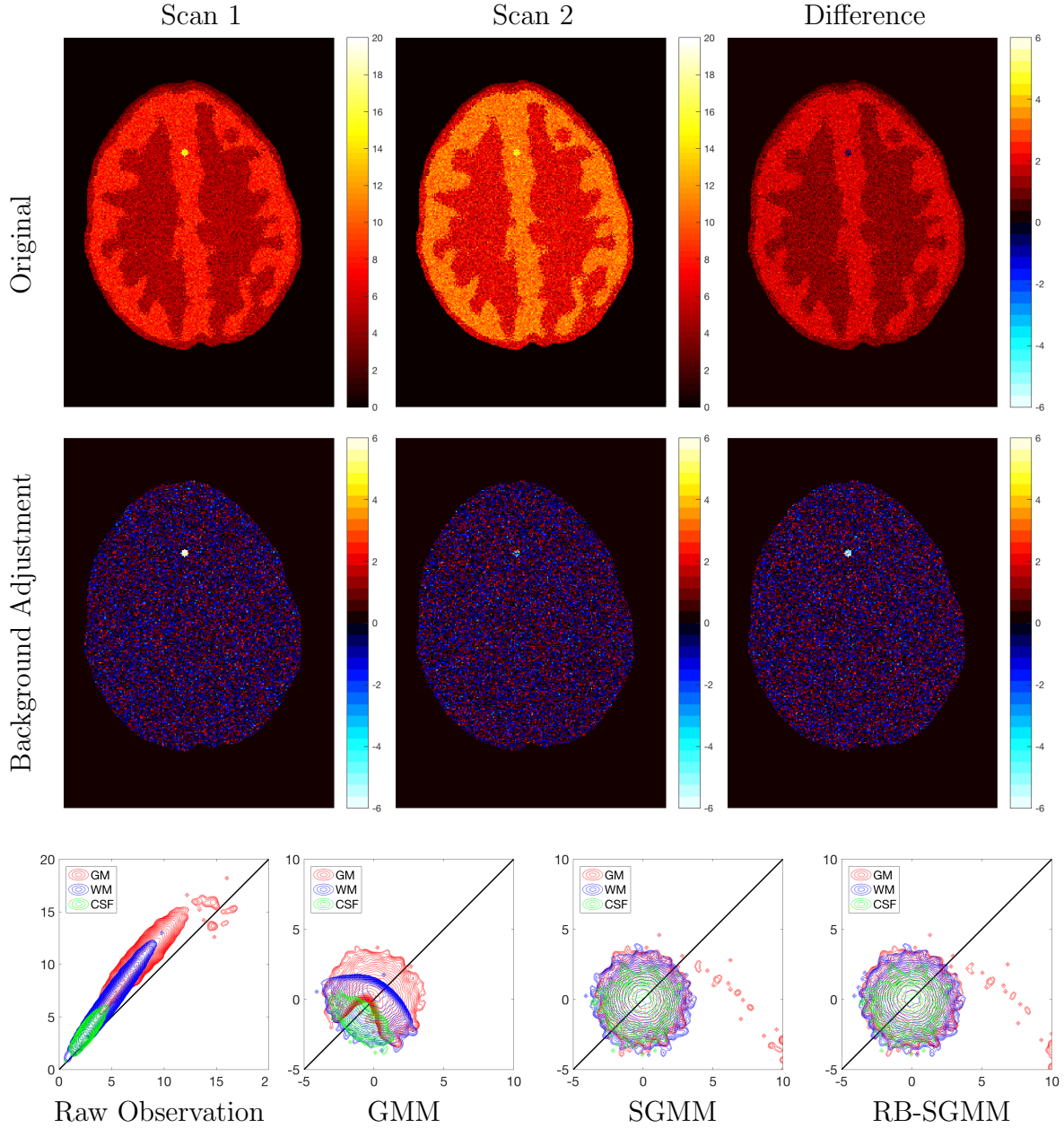
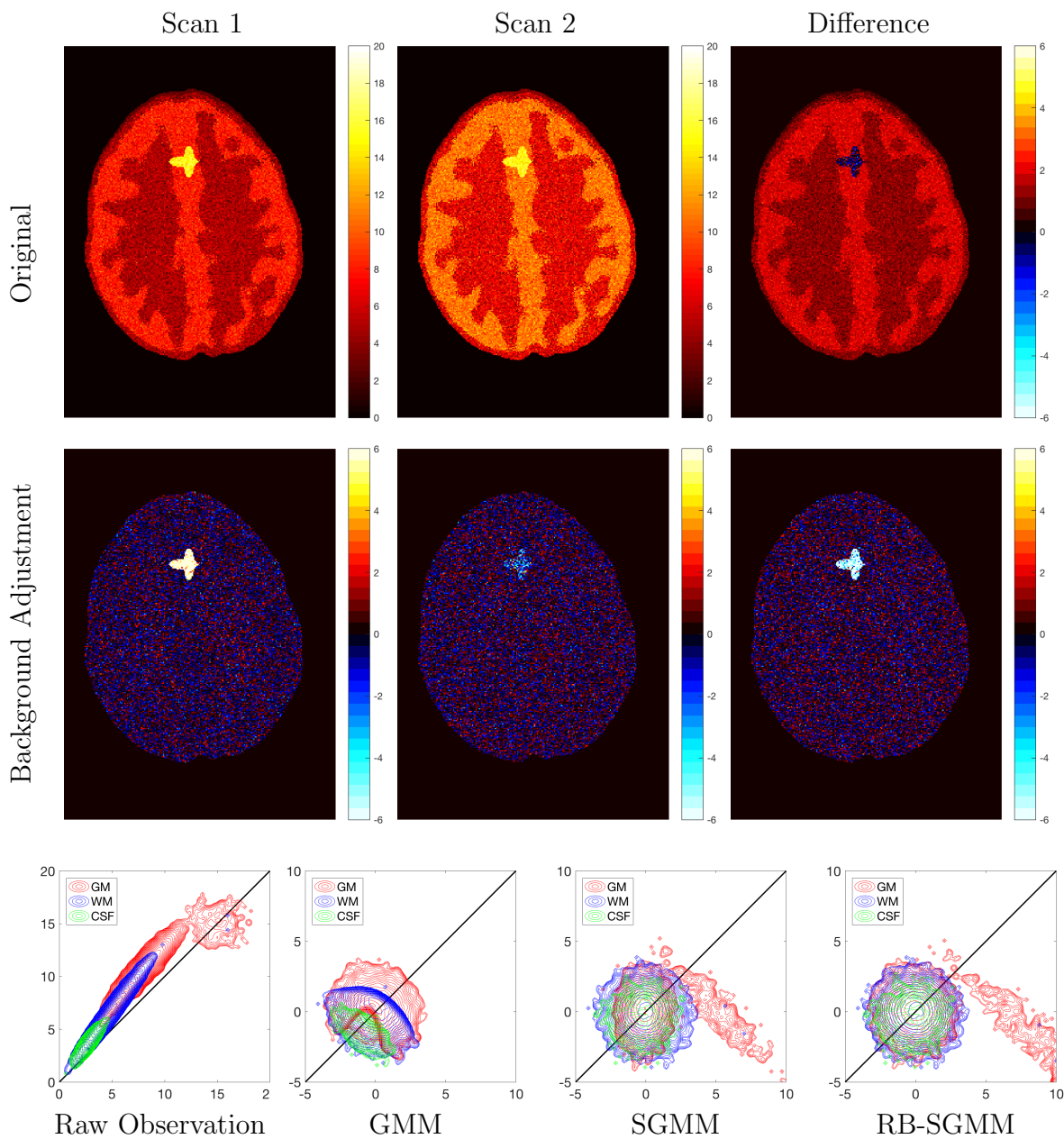


Figure 16: Simulated observations and background adjustment effects for Scenario B when the lesion is a union of two ellipses. The 1st row shows the simulated original scans and the corresponding contrast. The 2nd row shows the respective standardized images via background adjustment and their difference. The last row shows bivariate density contour plots of the observations with and without soft background adjustment within each class. The first column is for the original simulated observations, while the last three columns are the scores after background adjustment using the methods GMM, SGMM and RB-SGMM respectively.



RICE UNIVERSITY
DEPARTMENT OF STATISTICS
6100 MAIN ST, MS 138
HOUSTON, TX 77005, USA
E-MAIL: meng@rice.edu

UNIVERSITY OF CALIFORNIA, SAN DIEGO
DIVISION OF BIOSTATISTICS
9500 GILMAN DRIVE #0725
LA JOLLA, CA 92093, USA
E-MAIL: armins@ucsd.edu